Quality Of Service and MObility driven cognitive radio Systems

FP7-ICT-2009-4/248454

QoSMOS

D4.3

Flexible PHY concepts for white spaces – Final Report

Contractual Date of Delivery to the CEC:	30-June-2012
Actual Date of Delivery to the CEC:	12-July-2012
Editor: Rohit Datta (TUD)	
Authors:	Vincent Berg, Dominique Noguet (CEA), Atilio Gameiro (IT), Masayuki Ariyoshi, Yasunori Futatsugi (NEC), Mario Schühler (IIS), Zsolt Kollár, Péter Horváth (BME), Rohit Datta (TUD).
Reviewers:	Wolfgang Koenig (ALD), Dominique Noguet (CEA), Klaus Moessner (UNIS)
Workpackage:	WP4
Est. person months:	20 PM
Security:	RE
Nature:	P
Version:	1.0
Total number of pages:	**73**

Abstract:

Prospective modulation schemes for opportunistic, cognitive radio-based TV white space communications are considered. A discussion of filtering requirements to meet the current adjacent channel leakage regulations motivates the use of alternative multicarrier modulation schemes exhibiting well-controlled power leakage outside the useful bandwidth. In particular, novel windowed OFDM scheme is introduced together with new results on the performance of IA-PFT modulation scheme. Filter Bank Multicarrier and Generalized Frequency Division Multiplex are also considered and their performance is evaluated. Implementation aspects of Filter Bank Multicarrier are considered for the QoSMOS proof-of-concept prototypes.

Keyword list:

Cognitive Radio, OFDM, FBMC, IA-PFT, GFDM, System architecture, Physical layer, Multicarrier modulation

Abbreviations

AAF	Anti-Alias Filter
ACLR	Adjacent Channel Leakage Ratio
ADC	Analogue-Digital Converter
AGC	Automatic Gain Control
AIC	Active Interference Cancellation
AWGN	Additive White Gaussian Noise
BER	Bit Error Rate
BLER	Block Error Rate
BNC	Bussgang Noise Cancellation
BPF	Bandpass Filter
CC	Cancellation Carrier
CCDF	Complementary Cumulative Distribution Function
CEPT	European Conference of Postal and Telecommunications Administrations
CFO	Carrier Frequency Offset
CMT	Cosine Modulated Multitone
CP	Cyclic Prefix
CQI	Channel Quality Information
CSI	Channel State Information
DAB	Digital Audio Broadcasting
DAC	Digital-Analogue Converter
DSA	Dynamic Spectrum Access
DSO	Digital Switchover
DTT	Digital Terrestrial Television
DVB	Digital Video Broadcasting
EIRP	Effective Isotropic Radiated Power
ESM	Emission Spectrum Mask
FBMC	Filter Bank Multicarrier

FCC	Federal Communications Commission
FEC	Forward Error Correction
FD	Fixed Device
FFT	Fast Fourier Transform
FMT	Filtered Multitone
FPGA	Field Programmable Gate Array
GFDM	Generalized Frequency Division Multiplexing
IA-PFT	Interference Avoidance transmission by Partitioned Frequency- and Time-domain processing
IBO	Input Back-Off
ICI	Inter-Carrier Interference
IFFT	Inverse Fast Fourier Transform
IOTA	Isotropic Orthogonal Transform Algorithm
ISI	Inter-Symbol Interference
ISM	Industrial, Scientific and Medical
ITU	International Telecommunication Union
LAN	Local Area Network
LNA	Low Noise Amplifier
LTE	Long Term Evolution
MAC	Medium Access Control
MIMO	Multiple Input, Multiple Output
MMSE	Minimum Mean Squared Error
OFDM	Orthogonal Frequency-Division Multiplexing
OFDMA	Orthogonal Frequency-Division Multiple Access
OQAM	Offset QAM
PA	Power Amplifier
PAPR	Peak-to-Average Power Ratio
PHY	Physical Layer
PPD	Personal/Portable Devices

PPN	Polyphase Network
PSD	Power Spectrum Density
QAM	Quadrature Amplitude Modulation
QPSK	Quaternary Phase Shift Keying
SIC	Serial Interference Cancellation
SMT	Staggered Multitone
TMUX	Transmultiplexer
TRX	Transceiver
TVWS	TV White Space
TW	Time Windowing
UHF	Ultra High Frequency

Table of contents

List of figures

List of tables

1 Executive Summary

The objective of this deliverable is to summarize the new results achieved within QoSMOS to specify potential physical layer solutions; especially innovative modulation schemes with low out-of-channel radiation for opportunistic TV white space communications. This deliverable builds upon the work done in D4.2 and will give a detailed analysis on the achievable reduction of spectral leakage to adjacent legacy channels.

First, the currently known TV white space regulation rules are recalled[D4.2]. Based on these characteristics, recommendations are made for basic parameter selection for multicarrier modulation schemes. The current regulatory rules are also reviewed for out-of-channel leakage. The computational complexity of meeting these rules using conventional OFDM-based modulation and filtering is demonstrated.

Three improved OFDM-derivatives are considered first: a novel windowing scheme to OFDM to control the out-of-channel fall-off of the radiated signal; IA-PFT (Interference Avoidance transmission by Partitioned Frequency- and Time-domain processing) that is capable of producing a notch within its transmission spectrum by using a proper combination of windowing and cancellation carriers; and generalized frequency division multiplexing (GFDM) is described with its novel tail-biting cyclic prefix and pulse shaping filtering to produce a low out of band leakage. IAPFT and GFDM improve the adjacent channel leakage ratio to about -45 dB. Sensing a cognitive opportunistic signal is also of importance and hence simulations have been done on sensing GFDM signal and it is found out to give better ROC curves compared to OFDM.

Finally, a more general modulation technique is investigated to study their suitability for the physical layer of a TV white space communication system, namely Filter Bank Multicarrier (FBMC). This scheme addresses among others the good out-of-band radiation performance. Simulation results are shown to compare the signal characteristics and transmission performance of the proposed scheme.

As FBMC was selected for the modulation scheme to be used in QoSMOS demonstrations, practical synchronization aspects are covered, and novel peak-to-average power reduction techniques and equalization schemes are presented. As FBMC is constricted in frequency domain, in time domain, it is spread out and hence synchronization of FBMC signals was a problem. But recent efforts have produced efficient synchronization results with a patent already filed. Finally, progress on RF front-end design of the QoSMOS demonstrator transceiver is presented, and the effects of power amplifier-induced nonlinear distortion are predicted.

Recent results in lowering ACLR and synchronization in FBMC can be potential contributions in on-going standardization activities. Research work in lowering PAPR in FBMC will also impact standardization work.

2 Introduction

In today's scenario, radio spectrum is getting scarce and with opening up of some analogue TV bands, the intelligent use of the available spectrum by cognitive radio (CR) has become an important aspect of research in wireless communication. However, spectrum sharing between opportunistic users with licensed users needs to be done carefully so that incumbent user operation in adjacent frequency bands is not interfered with. One of the strict specifications for CR physical layer (PHY) modulation design is that the opportunistic signal should have extremely low out-of-band radiation, so that incumbent signals are not disturbed and co-existence is assured. Recent regulatory permitted interference level is around -60 dB. Moreover, to cope with spectrum fragmentation, the receiver should be able to aggregate several TV white spaces (TVWS) by a single wide band signal. Hence, innovative waveform design with a new multicarrier modulation capable of interference mitigation has emerged as a very important topic of research.

OFDM-based physical layer solutions of existing mobile access technologies, prominently 3GPP LTE and LTE-Advanced, are not suited for drop-in replacements in TVWS communications due to their high adjacent-channel leakage that doesn't comply with the existing European regulation. As pointed out by the P1900.7 contribution by [Berg2011], the LTE downlink waveform requires additional filtering to meet the -55 dB ACLR (Adjacent Channel Leakage Ratio) requirement which in turn leads to significant complexity increase in the implementation. Therefore, it is sensible to investigate alternative approaches as OFDM might not be the obvious choice in the specific case of TVWS operation under a low ACLR constraint. Efficient exploitation of fragmented spectrum is also difficult using a modulation scheme with slowly decaying of-out-channel radiation.

Neither of the above mentioned physical layer technologies are able to support all the QoSMOS scenarios efficiently. To resolve this, WP4 considers horizontal physical layer solutions where the same waveforms, parameterized according to the needs of the specific scenarios, can be re-used for various scenarios. Some of the proposed multicarrier modulation schemes lend themselves for spectrum pooling, and the proof-of-concept transceiver is designed to exploit this capability. Other proposed schemes possess excellent ACLR characteristics at manageable implementation complexity.

As one of the specified waveforms (Filter Bank Multicarrier) is being investigated and implemented within the project as proof-of-concept study, this document summarizes the current status of the radio frequency/baseband architecture study of the transceiver that will be used for the showcase implementations.

This document is organized as follows. In Chapter 3, the QoSMOS scenarios are characterized according to the dominant propagation conditions. Chapter 3 elaborates further on the requirements that are imposed on the physical layer of a TVWS-based opportunistic communication system. Some appropriate choices are also recommended for the key parameters of the physical layer in a waveform-agnostic manner. Chapter 4 recapitulates three modulation schemes that are slightly modified OFDM flavours: windowed OFDM, IA-PFT and GFDM. Chapter 5 presents the general multicarrier scheme with extremely low adjacent-channel leakage: Filter Bank Multicarrier. This scheme is more general than OFDM, and offers significantly better performance in terms of adjacent channel leakage. However, these schemes are not compatible with OFDM, hence they are not meant to be PHY replacements in legacy systems. Consequently, system designers can exploit their full potential in new, autonomous TVWS-based cognitive radio system. The PHY-related QoSMOS proof-of-concepts are FBMC-based.

Chapter 6 presents some preliminary results and performance studies on the QoSMOS proof-of-concept FBMC implementation from the transceiver point of view.

Finally, chapter 7 gives the conclusions that were drawn from the findings of the ongoing work, the chapter also points the way ahead to further work that should be undertaken to complement the reported findings.

3 Scenarios and physical layer requirements

The present chapter summarizes the most important scenario categories, as specified previously by QoSMOS WP2 D2.3 and in D4.2. Overview of femtocell, cellular extension and rural broadband scenarios are described.

3.1 Scenario descriptions

QoSMOS specified a set of working scenarios for cognitive applications (see [D1.3]). Three categories have been particularly in focus since the deliverable has been published, these are: "Cognitive Femtocell", "Cellular Extension" and "Rural Broadband" (or Backhaul). The smallcell/femtocell scenario (Figure 3-1), describes a user situation with low mobility, but high demands on throughput and QoS. It may also be described as a "hot spot" scenario. Femtocells are always connected to an infrastructure. Both indoor and outdoor deployments are possible.

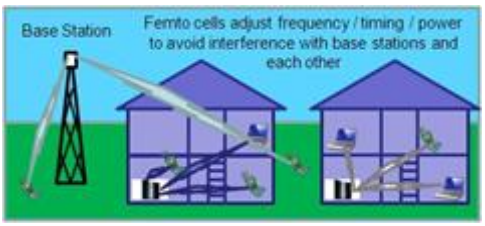

Figure 3-1: Overview of Femtocell scenario

"Cellular extension" in white space (Figure 3-2) is where mobile network operators (e.g. LTE-operators) will utilise white space spectrum in addition to their own licensed spectrum. The suitability of a spectrum band for this scenario depends on whether it is to be used for coverage or capacity enhancements.

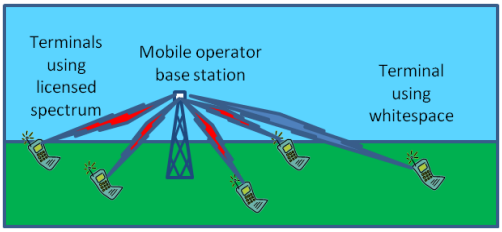

Figure 3-2: Overview of Cellular extension scenario

The Rural broadband scenario (Figure 3-3) typically includes properties of high dynamics and but where both terminals are of static nature this includes backhaul and rural broadband.

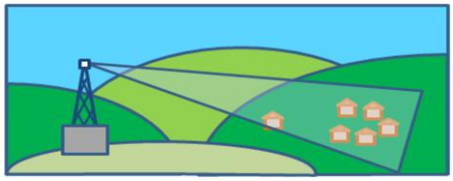

Figure 3-3: Overview of Rural Broadband scenario

The scenarios defined by QoSMOS are not limited to TVWS but since it is the most likely band where cognitive radio may occur in the near future and since physical layer specification requires propagation scenarios, it is suggested to analyse these scenarios in the case of TVWS.

With recent opening up of the analog TV bands in US[FCC1], opportunistic access of TV white spaces are possible and for that care needs to be taken so that legacy adjacent TV services are not interfered with by the opportunistic users. This is enforced by tight adjacent-channel leakage requirements by some regulators. Towards this end, OFDM is an initial choice for the cognitive radio PHY. But in an extremely fragmented spectrum, the side lobes of OFDM cause interference to the legacy incumbent TV signals. To avoid this, new post OFDM waveforms are needed for cognitive radio PHY design. These new waveforms need to be flexible multicarrier access to fill the fragmented spectrum holes. Therefore, the spectrum aggregation capabilities of the prospective physical layer techniques shall be considered as well.

3.2 Current TVWS regulation

In some countries, the Digital Switch Over (DSO) in TV bands has recently resulted in relaxed regulatory regimes subject to less stringent regulatory conditions, where unlicensed spectrum use is allowed, provided that non-harmful interference to incumbent systems is guaranteed. This move was first initiated in the USA, where the first proposed rules for the "Unlicensed Operation in the TV Broadcast Bands" were published as early as 2004 [FCC1]. A same initiative followed in the UK [OFCOM]. As a consequence, the unused TV spectrum, referred to as TV White Space (TVWS), has become one of the very first portions of the spectrum where the concepts of CR meet regulatory and actual deployment-driven requirement figures.

Many countries have therefore considered cognitive access to the TVWS but only the US and the UK have so far proposed parameter figures. These are the first elements of specifications for the CR in the TVWS. Some of these elements have already been described in previous deliverables and notably in [D1.3, D4.2] and are recalled in Table 3-1. Detailed description and reasoning for these values have been provided in D4.2.

Table 3-1: FCC and OFCOM TVWS transmit parameters

Parameter	FCC	OFCOM	Note
Power for FD in adjacent band	Not allowed	Not applicable	
Power for FD in non-adjacent band with geolocation capability	30 dBm	Not applicable	FCC: 36 dBm EIRP with a gain antenna
Power for PPD in adjacent band	16 dBm	4 dBm	Gain antenna not allowed
Power for PPD in non-adjacent band with geo-location capability	20 dBm	17 dBm	Gain antenna not allowed
Power for PPD in non-adjacent band without geo-location capability	17 dBm		
Out-of-band performance	< 55 dB	< -46 dBm	Relative to in-band power in the case of the FCC

For these reasons, a fair assumption is to consider that out of band adjacent channel leakage rejection should be at least 55 dB below the power emitted in band for the proposed physical layer waveform.

3.3 Challenges of a cognitive PHY for TVWS operation

Multicarrier modulation techniques in general and OFDM in particular, have developed as the most adapted techniques to broadband wireless communications. These waveforms have proven their capabilities in various applications and standards, and are commonly deployed in broadcast applications (DAB, DVB-T) as well as mobile wireless communications (WLAN, LTE). A relatively simple equalization and high bandwidth efficiency have been so far the main motivations for using OFDM when data is to be transmitted over a wireless multipath channel. Due to the narrowband subcarriers, the cyclic prefix in combination with channel coding, OFDM modulation techniques have led to very robust and reliable systems.

However, when it comes to spectral properties, OFDM waveform shows some limitations. An analytical expression for the power spectral density of the OFDM with cyclic prefix (CP-OFDM) waveform is proposed in [Waterschoot2010]. The result of the derived expression is recalled in (4-1):

$$P(f) = \frac{1}{T_s} \sum_k |G_k(f)|^2 \left[1 + 2 \frac{CP}{N + CP} \cos\left(\frac{2\pi f}{\Delta f} \right) \right] \qquad (4\text{-}1)$$

where N is the number of carriers in the OFDM waveform, CP, the duration of the cyclic prefix (in samples), Δf the carrier spacing and $G_k(f)$ the power spectral density of the pulse on carrier k. Assuming a brick-wall filter, $G_k(f)$ becomes the $sinc^2$ function centred on the active carrier. Figure 3-4 describes the power spectral density function of an OFDM waveform exhibiting similar parameters as defined in LTE: carrier spacing is set to 15 kHz, the size of FFT is set to 1024 and CP to 72 samples. Different active bandwidths corresponding to different number of active carriers are represented assuming an 8 MHz Emission Spectrum Mask (ESM).

The results highlight the necessity for a transmit filter cascaded after the modulator in order to limit the leakage of out-of-band signal power and meet the rejection level requirements of 55 dB. In order to understand the requirements on the transmit filter, we derive the rejection requirement on the transmit filter and then extrapolate the number of taps required for a finite impulse response implementation of the filter. The filter length is estimated using an equiripple lowpass implementation and should be applied to both real and imaginary components of the baseband signal. In order to keep the distortion of the OFDM signal to a reasonable level at the output of the transmitter, the ripple in the band is set to 0.5 dB, while the end of the passband is set to the limit of the occupied bandwidth.

The length and the complexity of the transmit filter increases dramatically as the guard band is reduced. A compromise between spectral efficiency and complexity has to be found.

When compared with the complexity of the OFDM modulation, the transmit filter introduces non-negligible level of added calculation. Assuming a split radix implementation, the OFDM complexity may be estimated by counting the number of real multiplication applied to each OFDM symbols and compare it with the equivalent complexity of the transmit filter:

$$\begin{aligned} C_{CP-OFDM} &= 2 \cdot \left(N \left(\log_2 (N) - 3 \right) + 4 \right) \\ C_{Tx-Filter} &= 2 N_{Filter} \cdot \left(N + CP \right) \end{aligned} \qquad (4\text{-}1)$$

Table 3-3 summarizes the complexity comparison using *N=1024* as the number of carriers. The length of the Tx filter relates directly to the proposed Tx filter in Table 3. Even if the number of taps in the Tx filter is very small (6 coefficients), the particularly efficient FFT algorithm facilitates that the order of complexity between the modulation and the filtering is equivalent.

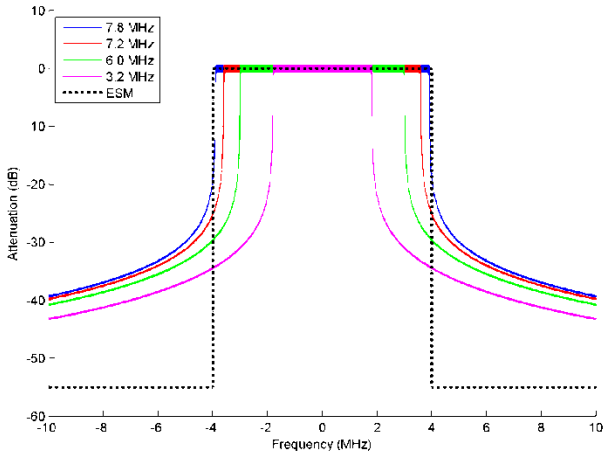

Figure 3-4: Power Spectral Density of CP-OFDM waveforms

Table 3-2 summarizes the results for the different scenarios of Figure 3-4.

Table 3-2: Complexity of transmit filter as a function of occupied bandwidth

Carrier Spacing	Occupied Bandwidth (MHz)	Number of Active Carriers	Guard Bandwidth (MHz)	Requirement on Tx Filter rejection to meet 55 dB rejection (dB)	Length of Baseband Tx Filter
15 kHz	7.8	520	0.1	35.4	230
	7.2	480	0.4	30.5	52
	6.0	400	1.0	25.4	18
	3.2	240	2.2	20.4	6

Table 3-3: Complexity comparison in number of real multiplications per symbol (N=1024) – ODFM TX Filter

Carrier Spacing	Occupied Bandwidth (MHz)	Complexity CP-OFDM	Complexity of Tx Filter for CP-OFDM
15 kHz	7.8	14 344	471 040
	7.2		106 496
	6.0		36 864
	3.2		12 288

It seems therefore that the simple approach of filtering OFDM to meet spectrum adjacent channel leakage requirements is not efficient.

On the other hand, aggressive filtering in order to reduce the adjacent channel leakage will result in decreased modulation accuracy. A compromise needs to be found between the filtering requirements and the modulation accuracy (e. g. the required error vector magnitude) that doesn't lead to significant deterioration of the bit error rate. Also, aggressive filtering requirements reduce the flexibility in multiple access scenarios, thus the OFDMA-based schemes are less attractive.

Finally, the potentially large peak-to-average power ratio (PAPR) should be mentioned as a well-known drawback in conjunction with multicarrier modulation. High PAPR can easily lead to power amplifier (PA) oversteering which in turn causes nonlinear distortion and consequently increases the amount of adjacent-channel leakage. Therefore, appropriate amplifier back-off and eventual predistortion shall ensure that nonlinear distortion is kept at an acceptable level. This aspect will be investigated in more detail in Chapter 5.

Based on the findings of this chapter and relevant works in D4.2, in cases where there is no need to adhere to legacy physical layer parameters, the studies are conducted on the following basis:

- The channel bandwidth is assumed to be 8 MHz.
- We propose to adopt 0.4 MHz guard bandwidth so that the occupied bandwidth is approximately 7.2 MHz.
- A subchannel spacing of 15 kHz is employed, which results in 480 subcarriers over the useful channel bandwidth.

3.4 Advantages of providing multiple PHY alternatives

The need for very low ACLR is the main motivation of QoSMOS to look for alternative modulation schemes that exhibit inherently low adjacent-channel leakage and this property can be retained even after experiencing some nonlinear distortion. Four multicarrier techniques are considered, in the order of increasing conceptual and computational complexity. Different schemes aim at different target, also from a standardization point of view. The improved OFDM-derivatives are intended to influence existing mobile standardization activities, specifically LTE, and propose modifications to the waveform that improve the spectrum pooling capabilities. The proposed modifications are of relatively low complexity and mitigate most of the previously mentioned filtering burden that would be necessary to limit the spectrum leakage. They provide a good compromise if some loss in the spectrum efficiency can be tolerated.

When QoSMOS considers more general multicarrier modulation schemes, the cognitive radio standardisation is specifically targeted to demonstrate that the loss in spectrum efficiency and increased implementation complexity due to filtering can be mitigated by employing modulation schemes that are designed from the ground up to provide the low ACLR values in the close vicinity of the useful band edge, thus eliminating the need for an overly wide transition band and the associated loss of efficiency, too.

An initial design is the cosine-modulated windowed OFDM system where the rate of fall of the side lobe power is increased. This is implemented with designing a soft-window technique based on the characteristics of functions with vestigial symmetry which are common in baseband data transmission. By using the vestigial symmetry and requiring at the extremes of the window and several null derivatives, it is possible to control a fast out-of-band decay.

An improvement on this above technique is the IA-PFT concept. Aiming to achieve deep suppression in the entire notch, an interference avoidance transmission by partitioned frequency- and time-domain processing (called as IA-PFT hereafter) for dynamic spectrum access is proposed, which synergizes combination effect of CC insertion and TW. IA-PFT is configured by the partition and a combination of the cancellation carrier (CC) insertion in the frequency domain and the time windowing (TW) processing in the time-domain.

Taking the idea of windowing techniques for pulse shaping of the symbols, a filter bank based multicarrier system is proposed. The distinctive feature of the FBMC technique is its ability to provide improved frequency selectivity through spectrally well-shaped prototype filters at the cost of a longer impulse response. Due to the frequency selectivity of the channel, FBMC only requires orthogonality for the neighboring sub-channels and offset quadrature amplitude modulation (OQAM) is used for this

purpose. The combination of filter bank with OQAM modulation guarantees the orthogonality without the need of a cyclic prefix (CP) as opposed to OFDM.

Evolving the idea of filter-bank modulation, a novel tail-biting cyclic prefix flexible multicarrier modulation technique called GFDM is designed. Here, a pulse shaping filter is used to shape the symbols and the out of band radiation is lowered compared to traditional OFDM out of band radiation at (-13 dB) depending on the choice of filters. GFDM can be thought of as an evolution of OFDM and FBMC with tail-biting cyclic prefix along with the pulse shaping ideas.

4 Physical layer techniques: evolution of CP-OFDM(A)-based schemes

This chapter presents three improvements to conventional OFDM. The first method employs specifically designed windows to force the side lobes of OFDM transmission to decay faster. The second scheme, IA-PFT, employs additional cancellation carriers in addition to time windowing to introduce a deep and uniform notch within the transmission bandwidth. The third method is GFDM, which employs time domain pulse shaping with tail-biting CP modulation.

4.1 Windowed OFDM

4.1.1 Description

Let us consider a scenario where opportunistic users share the spectrum with incumbents and both employ OFDM techniques for transmission of information. As shown the opportunistic terminals make use of the subcarriers that are momentarily unused by the incumbents as illustrated in Figure 4-1.

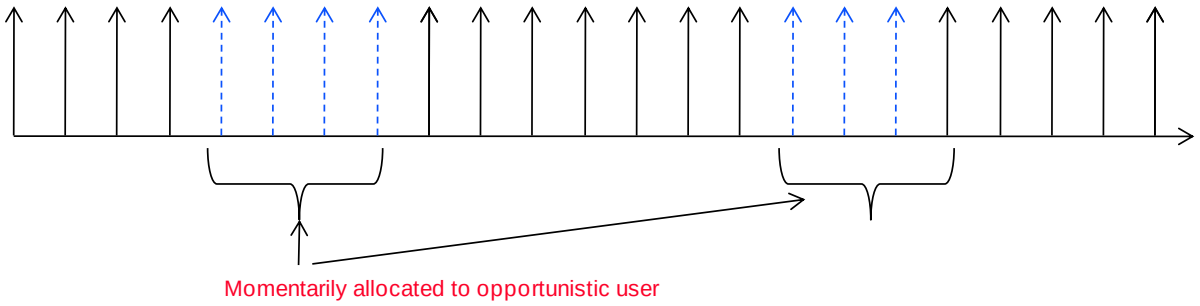

Figure 4-1: Illustration of the sharing of OFDM subcarriers in an incumbent user-opportunistic user coexistence scenario

To avoid harmful interference of opportunistic users on the incumbent it is desirable that the power spectral density (PSD) in incumbents' subcarriers exhibits a quick decay when out of band. The same principle applies to the interference of the incumbent over the opportunistic users, but since the incumbent is the licensee, it is the opportunistic user who has to guarantee non-harmful interference

In this section we propose and evaluate an enhancement to conventional OFDM, where modification from a rectangular to a smooth window allows high and controlled out-of band roll-off. A windowing technique in the time domain is used in IEEE802.11a [IEEE1999]. The block diagram of the transmitter is shown in Figure 4-2, where it can be seen the similarity with conventional OFDM, the only replacement being the windowing at the end of the chain, which requires a length of $2T_o$ for the symbol instead of T_o in the conventional OFDM using a rectangular window. The soft windowing which is based on the vestigial pulse formatting principles allows reusing most of the blocks of the transmitter which is of course useful for a smooth evolution.

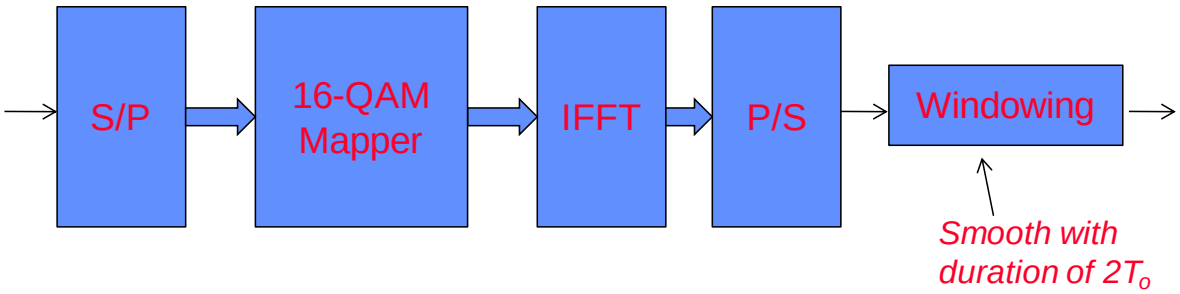

Figure 4-2: Block diagram of the transmitter

4.1.2 Characteristics of the transmitted signal

As referred in the previous section, the design of the soft-window Figure 4-2 is based on the characteristics of functions with vestigial symmetry which are common in baseband data transmission. By using the vestigial symmetry and requiring at the extremes of the window and several null derivatives, it is possible to control a fast out-of-band decay.

If a limited pulse (in time or frequency according to the domain we are dealing) has its first P derivatives at the extreme points equal to zero, then the asymptotic slope in the transform domain is at least of the order x^{-2P-2} [Bracewell99].

The assumptions for the signal (and consequently the window) design are:

- The normalized duration of the window is 2, which is equal to one of raised cosine (RC) 100%, i.e. there is a doubling of the window length compared to the conventional rectangular in order to ensure fast roll-off.
- the function can be decomposed in a cosine series of period 2, i.e.

$$w(t) = \sum_{k=0}^{N} a_k \cos(\pi k t) \qquad \text{for } -1 < t < 1 \tag{4-1}$$

It is clear from (5-1) that for N=1 and a_0=a_1=1/2 this reduces to the RC 100%.

The vestigial symmetry condition implies (e.g. [Schwartz90])

$$\begin{aligned}
&\sum_{k=0}^{N} a_k \cos(\pi k t) + \sum_{k=0}^{N} a_k \cos(\pi k (t-1)) = 1 \qquad \text{for } 0 < t < 1 \\
&\sum_{k=0}^{N} a_k \left(1 + (-1)^k\right) \cos(\pi k t) = 1 \quad \text{for } 0 < t < 1 \\
&\sum_{k=0}^{\lfloor N/2 \rfloor} 2a_{2k} \cos(\pi k t) = 1 \quad \text{for } 0 < t < 1
\end{aligned} \tag{4-2}$$

$$\Rightarrow \begin{cases} a_0 = 1/2 \\ a_{2k} = 0 \qquad k \geq 1 \end{cases}$$

It is easy to conclude from (5-2) that as long as $a_0 = \frac{1}{2}, a_{2k} = 0$ the vestigial condition is verified irrespective of the odd coefficients. Then

$$w(t) = \frac{1}{2} + \sum_{k=0}^{L} a_{2k+1} \cos(\pi(2k+1)t) \qquad \text{for } -1 < t < 1$$
$$L = \left\lfloor \frac{N-1}{2} \right\rfloor \tag{4-3}$$

where $\lfloor . \rfloor$ designates the lower integer.

Computing the derivatives, we get for the *p*th order one

$$w^{(p)}(t) = \begin{cases} (-1)^{\left(\frac{p+1}{2}\right)} \sum_{k=0}^{L} a_{2k+1} (\pi(2k+1))^p \sin(\pi(2k+1)t) & p \quad odd \\ (-1)^{\left(\frac{p}{2}\right)} \sum_{k=0}^{L} a_{2k+1} (\pi(2k+1))^p \cos(\pi(2k+1)t) & p \quad even \end{cases} \tag{4-4}$$

and at the end points (t=±1), one gets the values

$$w^{(p)}(1) = \begin{cases} (-1)^{1+\left(\frac{p}{2}\right)} \sum_{k=0}^{L} a_{2k+1} (\pi(2k+1))^p & p \quad even \\ 0 & p \quad odd \end{cases} \tag{4-5}$$

Therefore to have the first M derivatives null at the end points one needs to ensure that the series coefficients are chosen so that they verify (Subject to the conditions that w(0)=1)

$$\sum_{k=0}^{L} a_{2k+1} ((2k+1))^p = 0 \quad \text{for} \quad p = 2,4,..\lfloor M/2 \rfloor * 2 \tag{4-6}$$

As a design example, let us consider that we want the first two derivatives equal to zero (the third will also be null) and therefore design with two cosine terms. Then the conditions will be

$$\begin{cases} \frac{1}{2} + a_1 + a_3 = 1 \\ a_1 + 9a_3 = 0 \end{cases} \Leftrightarrow \begin{cases} a_1 = \frac{9}{16} \\ a_3 = -\frac{1}{16} \end{cases} \tag{4-7}$$

which leads to the pulse shown in Figure 4-3, where for comparison we also present the conventional RC 100%. We can observe that although smoother at the ends (since more derivatives are null) the new pulse has the energy more concentrated than RC 100%. Figure 4-4 illustrates the frequency domain behaviour where is clear the out-of-band decay at 90 dB/dec compared to the 10 dB/dec achieved with the rectangular and 60 dB/dec with RC 100%. The attenuation of the first lobe gives an improvement of 15 dB relative to conventional OFDM while for the second lobe we already get 55 dB attenuation.

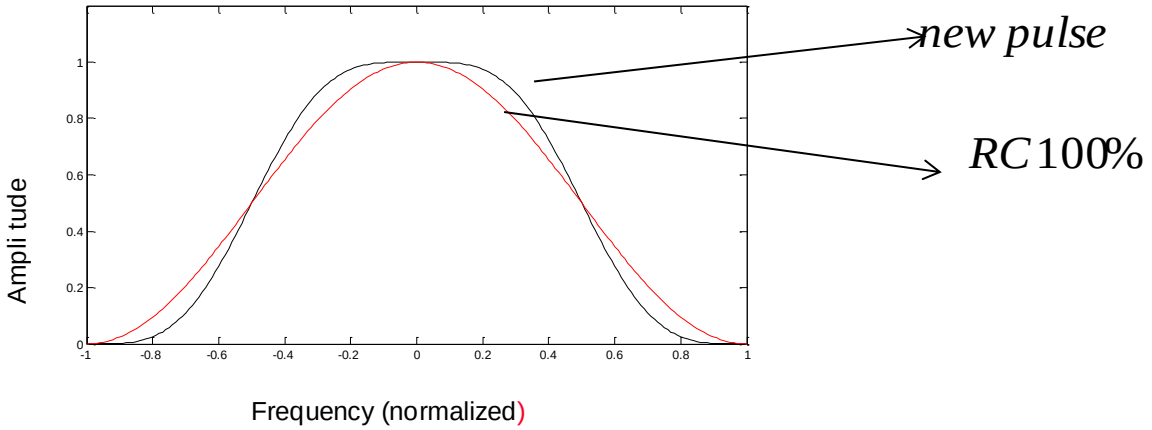

Figure 4-3: Comparison of RC 100% and pulse with tow null derivatives

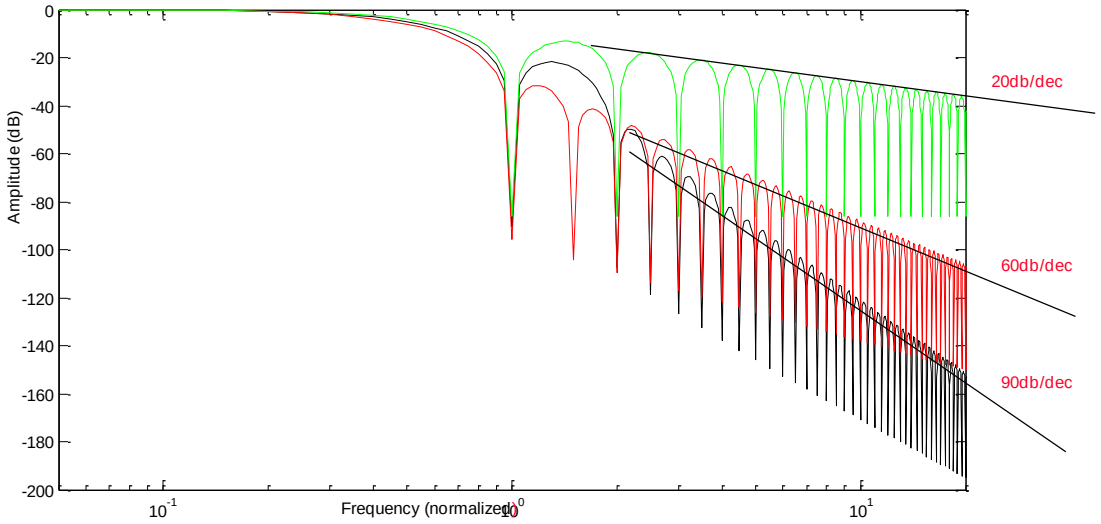

Figure 4-4: Frequency behaviour of the rectangular, RC 100% and pulse specified by (4.7)

4.1.3 Link-level performance

Let us first consider the asymptotic performance with RC 100%. To compensate for the extended length of the window one has to increase the modulation cardinality if one wants to preserve the bit rate. Assuming that with rectangular windowing the modulation scheme selected was QPSK, then with a RC 100% with the double of duration, the new modulation scheme should be one with 16 symbols e.g. 16-QAM. It is well known that the use of 16-QAM represents a degradation of 4 dB relatively to QPSK, while the use of a window that when normalized has values between 0 and 1 implies reduction of power.

In order to obtain the values for the asymptotic performance, we consider the expression of the analogue multicarrier signal, where f_0 represents the frequency of the first carrier

$$x(t) = \sum_{k=0}^{N-1} a_k e^{j2\pi\left(f_0 + \frac{k}{NT}\right)t} w(t) \quad (4\text{-}8)$$

Assuming independent data with unit power, one gets for the average power value:

$$\left\langle E\left[\left|x(t)\right|^2\right]\right\rangle_t = N\left\langle \left|w(t)\right|^2 \right\rangle_t \quad (4\text{-}9)$$

where $\langle . \rangle_t$ represents a time averaging operation and E[.] is the expectation operator. As

$$\left\langle \left|w(t)\right|^2 \right\rangle_t = \begin{cases} 1 & \text{Rectangular windowing} \\ 3/8 & \text{Raise cosine 100\% windowing} \end{cases} \quad (4\text{-}10)$$

it is easy to deduce that he performance gap relatively to OFDM with QPSK and rectangular windowing is $4 - 10\log_{10}\left(\frac{8}{3}\right) + 3 = 2.7\ dB$, where the value of -3dB comes from the fact that duration of the window is doubled. Therefore the price to provide an asymptotic decay of 60dB/dec instead of 20dB/dec is a power penalty of 2.7 dB. It is worth to note that the gap will still be slightly lower if one accounts for the cyclic prefix and pilots, which has not been done here.

Let us now consider the performance with the smoother pulse defined by (5-7). In this case we get for the average power of the windowing function $\left\langle \left|w(t)\right|^2 \right\rangle_t = 105/256 \approx 0.41$, which is slightly higher than the one obtained with RC 100% (0.375 from 5.10)), and gives us an asymptotic performance gap of $4 - 10\log_{10}\left(\frac{256}{105}\right) + 3 = 2.8\ dB$.

4.1.4 Conclusions

The design principles for windowed OFDM technique considered in this section have shown that in a simple modification of the OFDM conventional chain through a different windowing allows to control the out of band roll-off of the pulse. That is of interest for the incumbent-opportunistic user paradigm, where the opportunistic user should not cause harmful interference on the primary. The combination of OFDM which is useful to identify vacant carriers, and controlled windowing which ensures no spill over of energy over used carriers, is a good solution to reuse significant part of the design used in conventional OFDM with the goal of very low energy leakage. As an example designing for the first two derivatives to be null, one gets an improvement of 15dB relatively to conventional OFDM in the first lobe, while the next lobes already achieve the 55dB attenuation criteria. These benefits come at the cost of a performance penalty which is in the order of 2.8 dB if one wants to keep the same bit rate.

4.2 IA-PFT

4.2.1 Concept of IA-PFT

For an opportunistic OFDM-based dynamic spectrum access (DSA) system, it is important to reduce the undesired out-of-band spectrum emission so that the system can coexist with incumbent system. A windowing technique in the time domain is used in IEEE802.11a [IEEE1999], which is referred to as time windowing (TW). The TW approach is able to significantly reduce out-of-band emission for the centre of the notch. Alternatively, Active interference cancellation (AIC) is known as a method of inserting interference suppression carriers into the original transmission sub-carriers in order to suppress the side-lobes in the interference avoidance notch [Yam2004]. Similar approaches, called as

cancellation carrier (CC) insertion have been studied (the CC insertion is considered as a kind of AIC). The CC insertion is able to significantly reduce out-of-band emission at the edge of the notch. A simple serial combination of CC insertion and TW has been investigated in [Bran2005]. However, this approach cannot achieve enough interference suppression, because the suppression effect by the CC insertion at the edge is insufficient due to a cyclic extension in the TW processing.

Aiming at achieving deep suppression in the entire notch, we propose an interference avoidance transmission by partitioned frequency- and time-domain processing (called as IA-PFT hereafter) for DSA, which combines effect of CC insertion and TW [D4.1]. Here, 480 kHz of bandwidth notch for a wireless microphone is assumed. IA-PFT is configured by a combination of CC insertion in the frequency domain and the TW processing in the time-domain: that is, the CC insertion and the TW are separately applied to the transmitted sub-carriers. Hence, the suppression effect by the CC insertion is not violated by the TW. For adequate combined effect of CC insertion and TW, the proposed IA-PFT allocates the sub-carriers suppressed by the CC near the notch. Furthermore, the proposed IA-PFT employs the TW to the rest of the sub-carriers.

4.2.2 Characteristics of the transmitted signal

4.2.2.1 Transmission method

Figure 4-5 shows a transmitter structure of IA-PFT. The transmitter employs two IFFT modules for the shared band transmission signal. The transmission bit stream is modulated and divided into a time-windowing-processed signal stream and a CC-processed signal stream at the sub-carrier mapping. A cyclic prefix and a cyclic postfix (commonly abbreviated as CP) are respectively appended to the head of the OFDM symbols and to the tail of the OFDM symbols [IEEE1999]. The reason for appending the CPs is to smooth the OFDM symbols without shaping original rectangular OFDM symbols to avoid signal distortion. As for the CC-processed signal stream, CCs are inserted into the original transmitted sub-carriers in the frequency domain to suppress undesired spectrum emission near the edge of notch. A Zero Padding (ZP) is appended to the head of the OFDM symbols. The reason of the ZP appendix is to match the side-lobes of the CCs and those of the transmission sub-carriers, and consequently to enhance suppression effect by CC insertion.

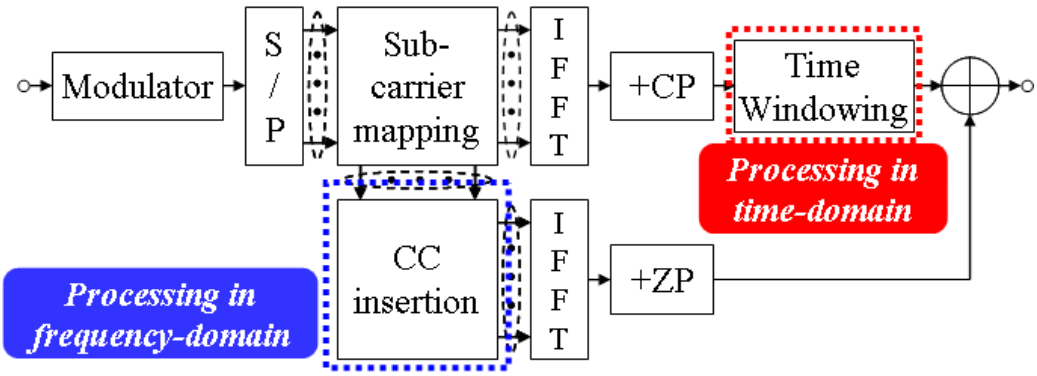

Figure 4-5: Transmitter structure of IA-PFT

Figure 4-6 shows the sub-carrier allocation of IA-PFT. CCs are inserted close to the interference avoidance notch (N_i). The CCs are calculated to suppress side-lobes on a null band ($N_{i\_partial}$) from the interference sources covered by the CC-processed signal (Q sub-carriers). The null band is set to the vicinity of the CCs in the notch. Aiming at achieving adequate synergy effect of TW and CC insertion,

the sub-carriers of the low-priority system suppressed by the CCs are allocated near the CCs, and the rest of the sub-carriers for the low-priority system are suppressed by the TW.

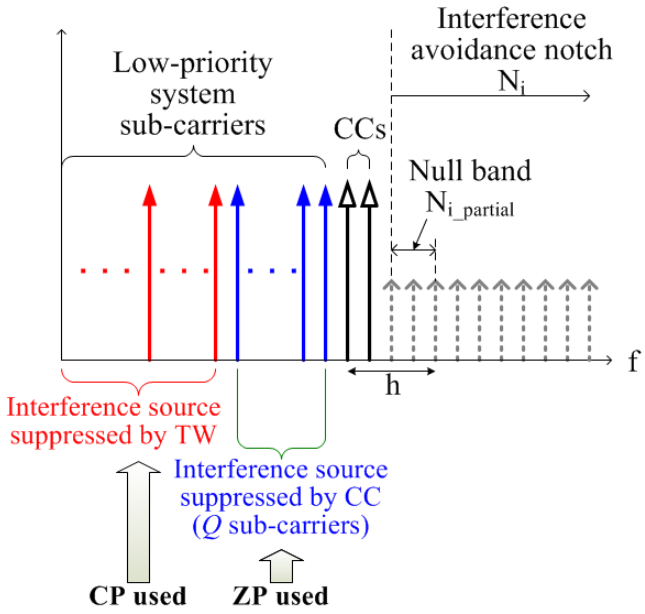

Figure 4-6: Sub-carrier allocation

4.2.3 Link-level performance

4.2.3.1 Power spectrum density

The major parameters (based on 3GPP Evolved UTRA [TS36.201][TS36.211]) used in the power spectrum density are listed in Table 4-1.

Table 4-1: Simulation parameters for power spectrum density

Parameter	Assumption
FFT size	1024
Number of sub-carriers	564
CP (ZP) sample	72
Sub-carrier spacing	15 kHz
Modulation	QPSK

Figure 4-7 shows the transmission spectrum in the case of the interference avoidance for the wireless microphone. In the figure, the performance of IA-PFT is compared with those of the normal OFDM, TW [IEEE1999], CC insertion [Yam2004] and the serial combination of CC insertion and TW (shown as CC+TW serial) [Bran2005]. The number of sub-carriers for the notch (N_i) was set to 32. For the TW, the number of sub-carriers for the notch was set to 34 to fit the same spectrum efficiency of the CC insertion and IA-PFT. As for IA-PFT, interference suppression partitioned by the CC insertion and TW was applied to each spectrum edge. The parameter Q was set to 15. QPSK modulation scheme was assumed. From the simulation results, the TW and CC+TW serial cannot achieve the high suppression effect near the transmitted sub-carriers in the notch. Meanwhile, the CC insertion cannot achieve the high suppression effect in the central portion of the notch. For IA-PFT, the maximum

suppression effect of power spectrum density is about 10 dB higher than attained by the CC+TW serial. Furthermore, IA-PFT can obtain the maximum suppression effect of 14 dB compared with the normal OFDM.

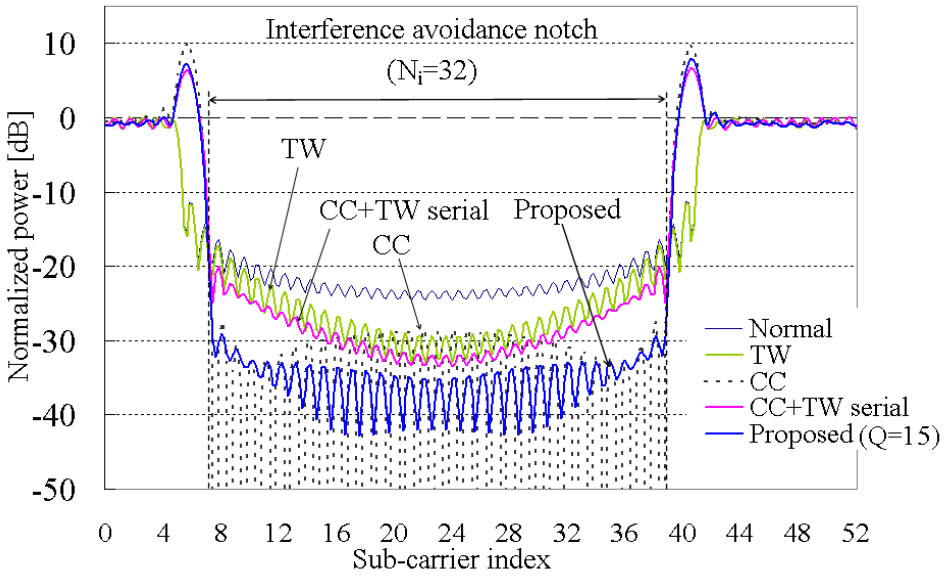

Figure 4-7: Power Spectrum Density

4.2.3.2 Transmission performance

The major parameters used in the transmission performance are listed in Table 4-2.

Table 4-2: Simulation parameters for transmission performance

Parameter	Assumption
FFT size	1024
Number of sub-carriers	564 (N_{notch}=1), 456 (N_{notch}=4)
CP (ZP) samples	72
Sub-carrier spacing	15 kHz
Channel coding / decoding	Turbo coding (K=4) / Max-Log-MAP decoding
Modulation scheme	QPSK, 16QAM (R=1/2, 3/4)
Channel model	Typical Urban
Maximum Doppler frequency	f_D=20 Hz
Channel estimation	Ideal
Number of receiver antennas	1

Figure 4-8 shows the block-error-rate (BLER) performance of IA-PFT with a condition of coding rate of 1/2 (R=1/2) and a single notch (i.e., the number of notches, N_{notch}, equals to 1). As comparison methods, the CC [Yam2004], TW [IEEE1999] and CC+TW serial [Bran2005] were also evaluated. The required E_b/N_0 at BLER of 10^{-2} for IA-PFT is almost same as that in the case of the TW and

CC+TW serial. However, the BLER performance of the CC is worse than that of IA-PFT, because the inter-carrier-interference (ICI) is induced by the ZP. The difference between transmission performance of IA-PFT and of the TW is very small in the case of 16QAM.

Figure 4-9 shows the BLER performance of IA-PFT with R=3/4 and N_{notch}=4. This is a kind of severe conditions for IA-PFT such as higher coding rate and multiple active channels used by wireless microphone. The difference between transmission performance of IA-PFT and of the TW is 0.5 dB in the case of 16QAM. This performance impairment for IA-PFT is caused by the ZP appended sub-carriers. Nevertheless, the loss of the required E_b/N_0 can be seen as small because the maximum suppression effect attained by 12 dB compared to that of the TW.

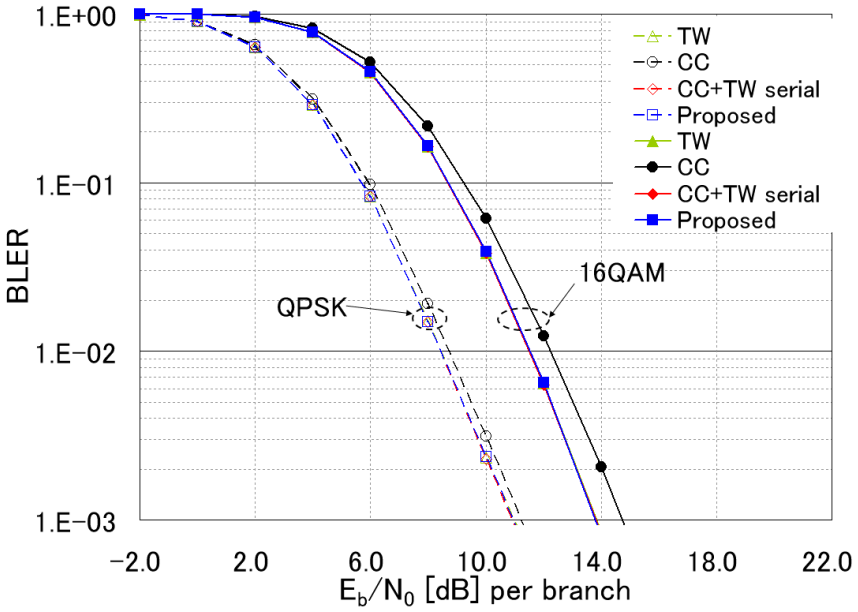

Figure 4-8: BLER performance (R=1/2, N_{notch}=1)

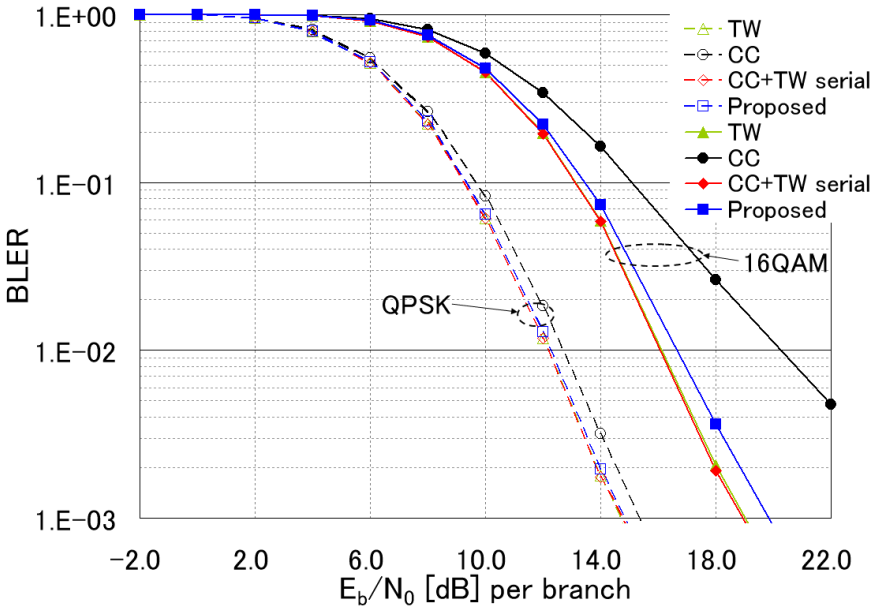

Figure 4-9: BLER performance (R=3/4, N_{notch}=4)

4.2.3.3 PAPR performance

Figure 4-10 shows PAPR of IA-PFT when 16QAM R=3/4 and N_{notch}=4 are assumed. In this evaluation, the simulation parameters were set to same values as Figure 4-9. From the simulation result, PAPR of CC insertion is increased by 0.4 dB compared to the TW when Complementary Cumulative Distribution Function (CCDF) is equivalent to 1%. The reason of the increase of PAPR for CC insertion is that ZP is used for all the sub-carriers. On the other hand, PAPR of IA-PFT is almost same as that of the TW since ZP is partially used for the sub-carriers.

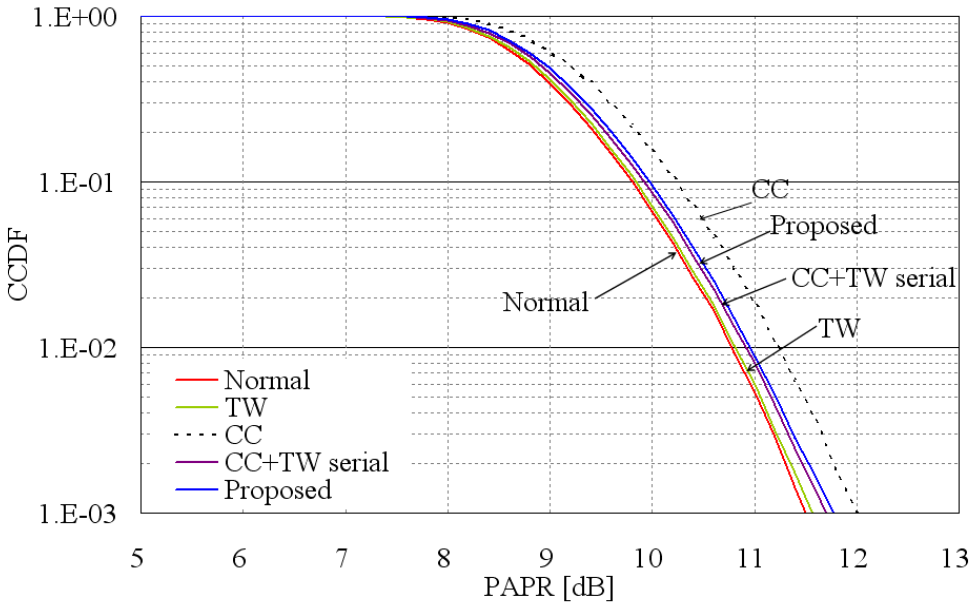

Figure 4-10: PAPR performance (R=3/4, N_{notch}=4)

4.2.3.4 Computational Complexity

For the transmitter side of IA-PFT, additional complexity is required due to twin-IFFT scheme. The number of multiplications per OFDM symbol is expressed as

$$\mu_{IA-PFT}^{Tx} = N\log_2 N + 2L_{OV} + N_{CC}N_{edge}Q \qquad (5\text{-}1)$$

where N, L_{OV}, N_{CC}, N_{edge}, and Q are respectively FFT size, the number of overlapping samples for TW, the number of CCs, the number of spectrum edges, and the number of sub-carriers processed by CC. The complexity analysis result is listed in Table 4-3. It is defined that $N_{effective}$ represents the number of effective sub-carriers. The complexity of IA-PFT increases compared with that of TW. However, it can be seen that the increase of complexity does not affect significant impact on the transceiver if all of the baseband processing is considered. It is also noted that a normal OFDM receiver can be used for IA-PFT receiver which does not require any interference cancellation processing.

Table 4-3: Complexity analysis

Transmission scheme	Complexity
NC-OFDM	$\mu_{NC}^{Tx} = \frac{N}{2}\log_2 N$
TW	$\mu_{TW}^{Tx} = \frac{N}{2}\log_2 N + 2L_{OV}$
CC	$\mu_{CC}^{Tx} = \frac{N}{2}\log_2 N + N_{CC}N_{edge}N_{effective}$
CC+TW serial	$\mu_{CC+TW}^{Tx} = \frac{N}{2}\log_2 N + 2L_{OV} + N_{CC}N_{edge}N_{effective}$
IA-PFT	$\mu_{IA-PFT}^{Tx} = N\log_2 N + 2L_{OV} + N_{CC}N_{edge}Q$

4.2.4 Conclusions

An advanced interference suppression method called IA-PFT was presented. The structure of IA-PFT features a combination of parallel processing of transmit sub-carriers in frequency domain (CC insertion) and in time domain (TW). IA-PFT allocates the sub-carriers suppressed by the CCs near the notch. This contributes to achieve high suppression effect near the edge of the notch. Besides, IA-PFT applies the TW to the rest of the sub-carriers. This contributes to achieve high suppression effect at the centre of notch. Computer simulations showed that IA-PFT outperforms the conventional methods in terms of interference suppression effect. Moreover, negative impacts of IA-PFT on transmission performance and PAPR performance are low enough. It is therefore concluded that IA-PFT is a promising candidate for OFDM-based DSA systems.

4.3 Generalized Frequency Division Multiplexing

GFDM is an innovative multicarrier modulation technique which is suitable for cognitive PHY in fragmented white spaces. Unlike OFDM, where we have rectangular pulse shaping, here in GFDM, we have an added flexibility of choosing a suitable pulse, like Root Raised Cosine (RRC) or Raised Cosine (RC). This pulse shaping technique brings the advantage of extremely low out-of-band radiation of the opportunistic signal into the incumbent legacy band, as RRC pulses have lower side lobes compared to rectangular pulses in OFDM. In extremely fragmented radio spectrum, reducing the side lobes is of importance, as it avoids causing interference to the legacy primary users.
GFDM is OFDM like multicarrier system with an added flexibility of choosing the pulse shape. With RRC pulse shaping, the out of band leakage reduces compared to OFDM. In FBMC, using a special spectrally shaped pulse decreases the out of band leakage. Compared to GFDM, where QPSK/QAM signaling is used, FBMC uses OQAM to get rid of the in-band interferences. FBMC has the lowest out of band interferences of all the multicarrier modulation PHY designs.

As described in [Fettweis2009], GFDM is a multicarrier system incorporating a tail-biting technique. By applying the Tx/Rx filters via circular convolution, the length of the transmitted signal is kept independent from the length of the pulse shaping filters [Nicola2011].

In the transmitter part of the system in Fig. 4-11, the binary data is QPSK/QAM modulated and then the transmit pulse shaping filter shapes the modulated data. Then after sub carrier up-conversion the transmitter transmits the modulated signals with cyclic prefix.

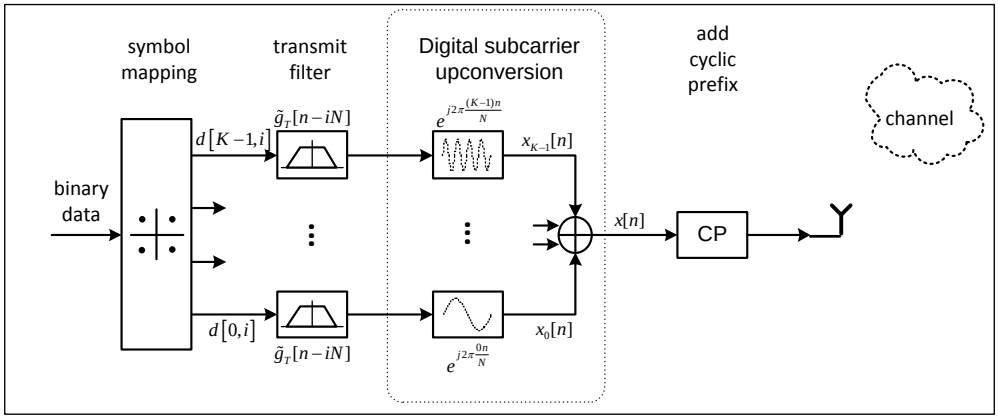

Figure 4-11: GFDM transmit system model

In the receiver part of the system, Fig. 4-12, the CP is removed and then after equalization, sub carrier down-conversion is performed. The received signal is then passed through the matched received pulse shaping filter, followed by a sampler and a detector to get back the binary data.

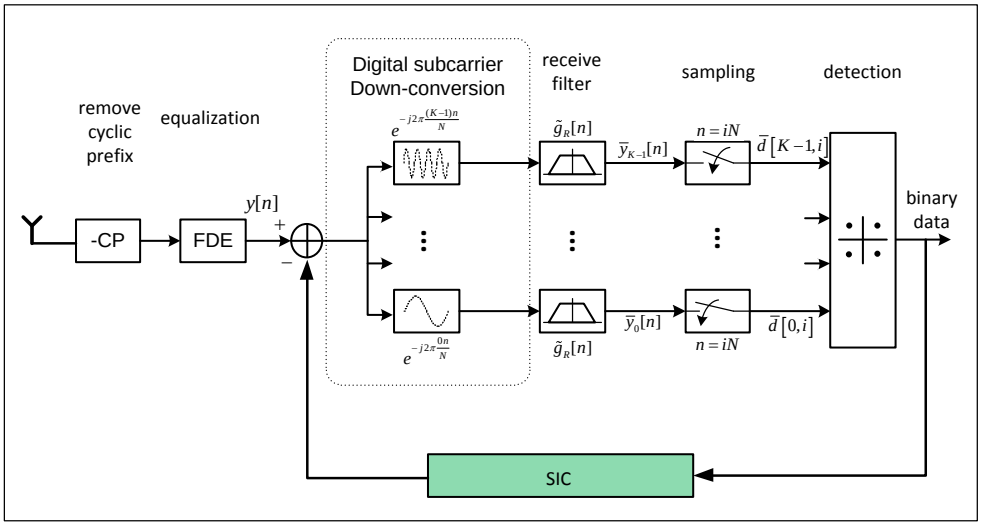

Figure 4-12: GFDM receive system model

The receiver also shows the serial interference cancellation scheme that has been implemented to improve the performance of the GFDM system.

As shown in [Fettweis2009], since here we have less number of subcarriers compared to OFDM, the PAPR of this system is better than that of OFDM by about 1 dB at 1% CCDF. Different pulses like RRC introduces non-orthogonality and causes ICI between the subcarriers, the BER curve of GFDM is degraded compared to theoretical AWGN BER curve. As shown in the next section, GFDM can achieve good performance with simple equalization schemes, demanding reasonable complexity increase in the equalizer.

The out-of-channel leakage of GFDM is shown in Fig. 4-13. 600 subcarriers are considered out of which 564 subcarriers are active and the remaining 36 subcarriers are made OFF. 1024 point FFT is considered to get the power spectral density plot. Compared to OFDM's -13 dB, it is observed that the second power lobe profile is at -25 dB for GFDM.

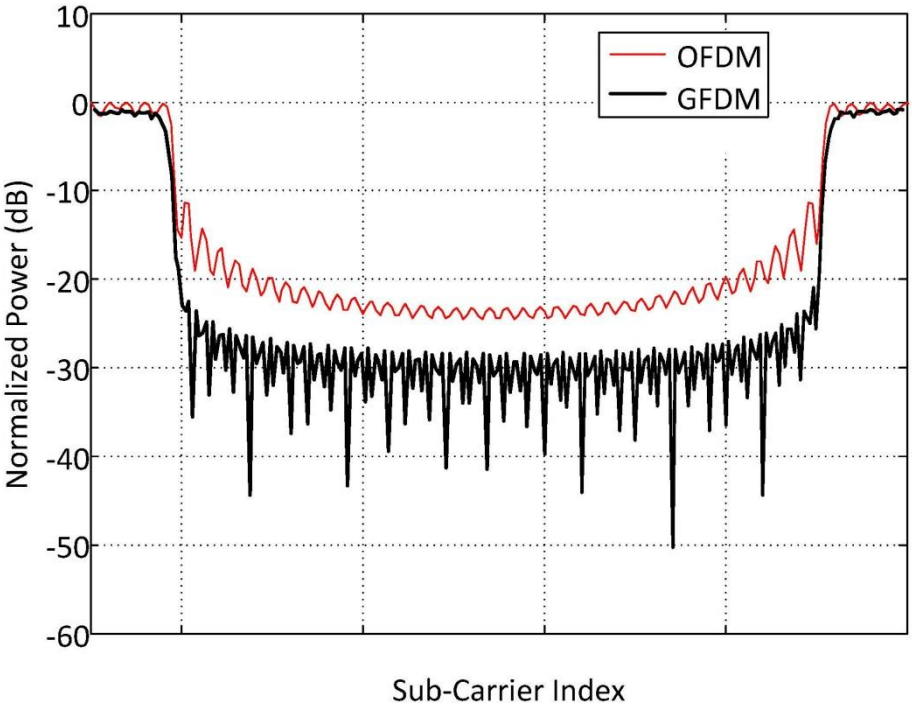

Figure 4-13: GFDM out-of-channel leakage

4.3.1 GFDM-ICI Cancellation Scheme

A simple inter carrier interference cancellation scheme, Serial Interference Cancellation (SIC) can improve the performance of the GFDM system. In our simulation setup we have considered AWGN channel, and RRC pulse. The interference under consideration is the self inter carrier interference that crops up because of the pulse shaping filters. The significant contributions of the interferences are from the adjacent subcarriers. One simple way to cancel out the effect of this interference is to perform Serial Interference Cancellation (SIC) [Clark72]. Performance results are obtained through simulation. The parameters are tabulated in Table 4-4. The GFDM system is simulated in an additive white Gaussian noise (AWGN) channel with uncoded transmission. QPSK and 16 QAM modulation schemes have been implemented with number of subcarriers, K = 64 and samples per symbol, N = 64. The block size considered is M = 15. Root-raised-cosine (RRC) filters are chosen with roll-of-factor α = 0.3. As an AWGN channel environment is simulated, cyclic prefix is not considered in the simulation setup.

Table 4-4: GFDM simulation parameters

Modulation Scheme		2(QPSK), 4(16 QAM)
Samples per symbol	N	64
Subcarriers	K	64
Block size	M	15
Filter type		RRC
Roll-off factor	α	0.3

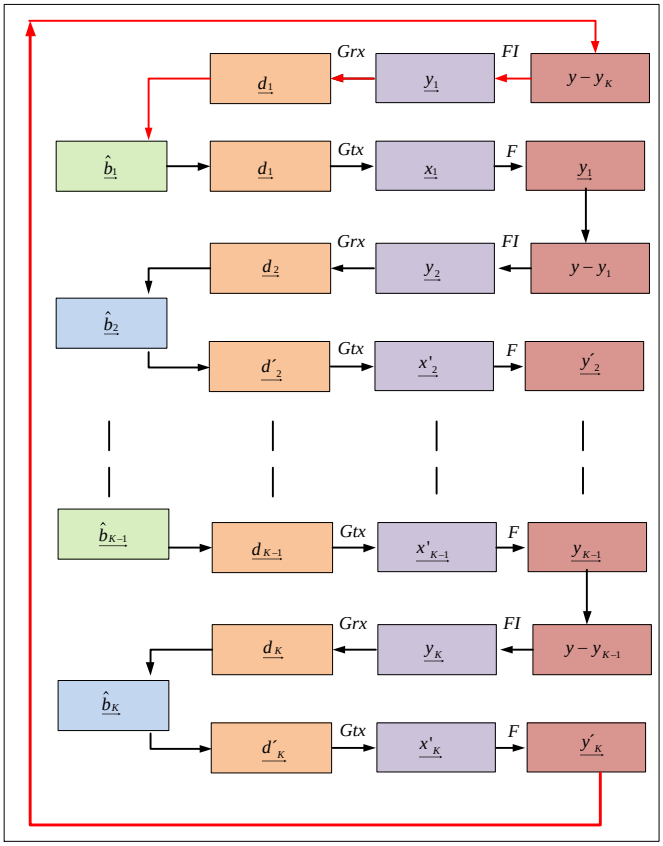

Figure 4-14: SIC block diagram

Once a particular subcarrier is detected, it is modulated again and pulse shaping is done before it is up-converted, to generate the approximate transmitted signal. Then this estimate of the transmitted signal is subtracted from the received signal to cleanse the effect of that subcarrier on the adjacent one.

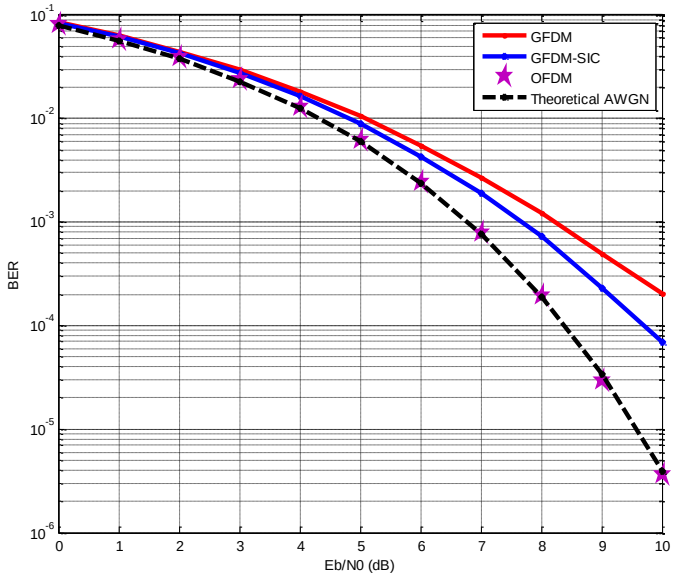

Figure 4-15: QPSK GFDM SIC BER performance vs. theoretical AWGN

Then the entire receiver processing is done, namely subcarrier down-conversion, receive filtered and then sampled. Then the next subcarrier is detected and as usual the above mentioned methodology is applied to cleanse the effect of the adjacent subcarriers on the carrier of interest.

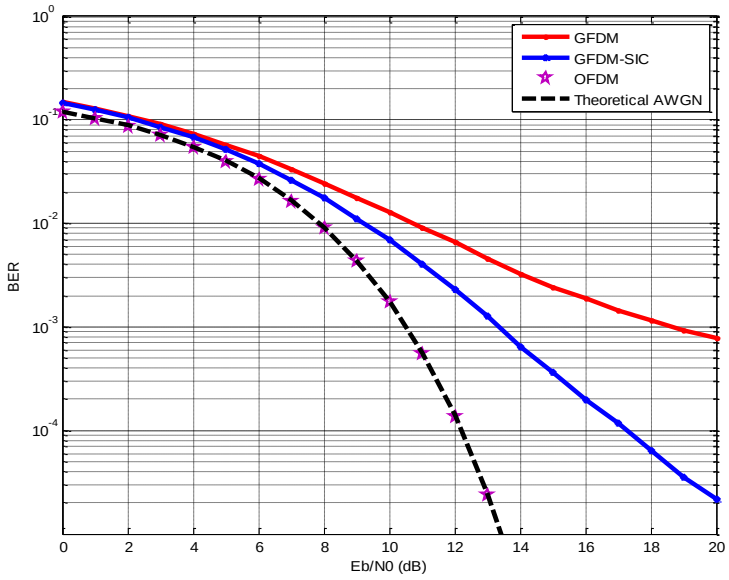

Figure 4-16: 16QAM GFDM-SIC BER performance

The GFDM BER performance improvement is shown for QPSK and for a 16 QAM constellation. Thus we see, SIC improves the BER performance, but it is still a bit worse than the theoretical OFDM-AWGN curve, although the performance is better compared to the results in [Fettweis2011]. The GFDM BER performance can be further improved by implementing a double sided interference cancellation scheme.

4.3.2 Double sided ICI cancellation

In this double sided Serial ICI cancellation, the two adjacent subcarriers are detected. After that the data on these two subcarriers are modulated again and pulse shaping is done before it is up-converted, to generate the approximate transmitted signal, as shown in Fig.4-17. Then this estimate of the transmitted signal is subtracted from the received signal to cleanse the effect of that two adjacent subcarrier induced ICI on the subcarrier of interest.

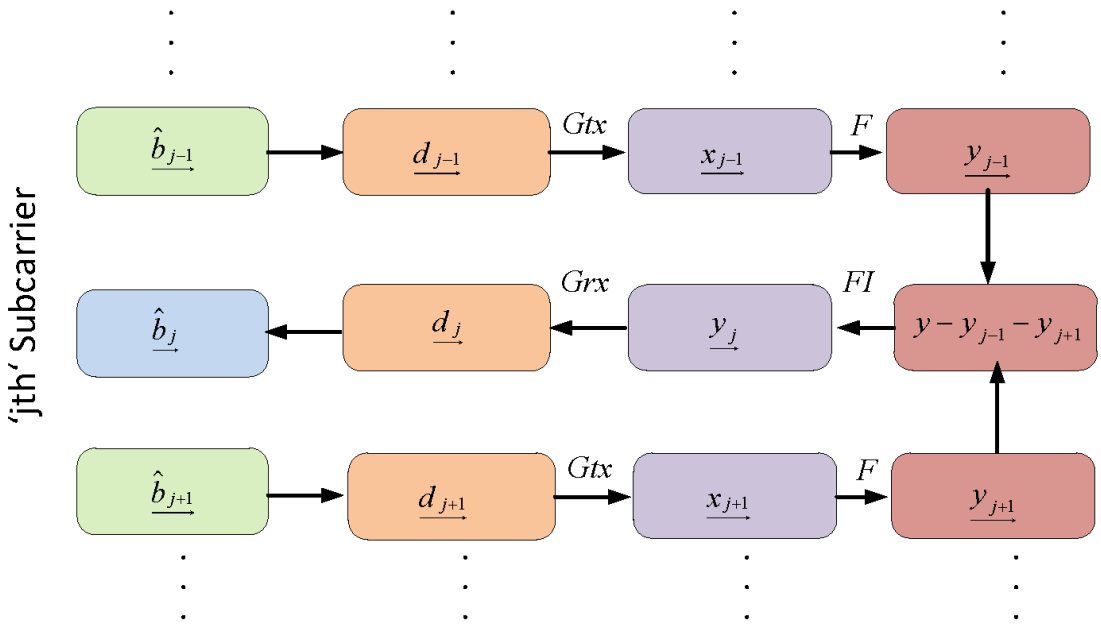

Figure 4-17: Double-sided SIC block diagram

Then the entire receiver processing is done, viz. subcarrier down-conversion, receive filtered and then sampled. Then the next subcarrier is detected and as usual the above mentioned methodology is applied to cleanse the effect of the adjacent subcarriers on the carrier of interest.

The BER performance the GFDM system with double sided serial interference cancellation is shown in Fig. 4-18. Here it is observed that the BER performance of the GFDM has improved and it is now following the theoretical AWGN curves. The double sided SIC clearly removes all the self-ICI that pulse shaping introduces in to the GFDM system.

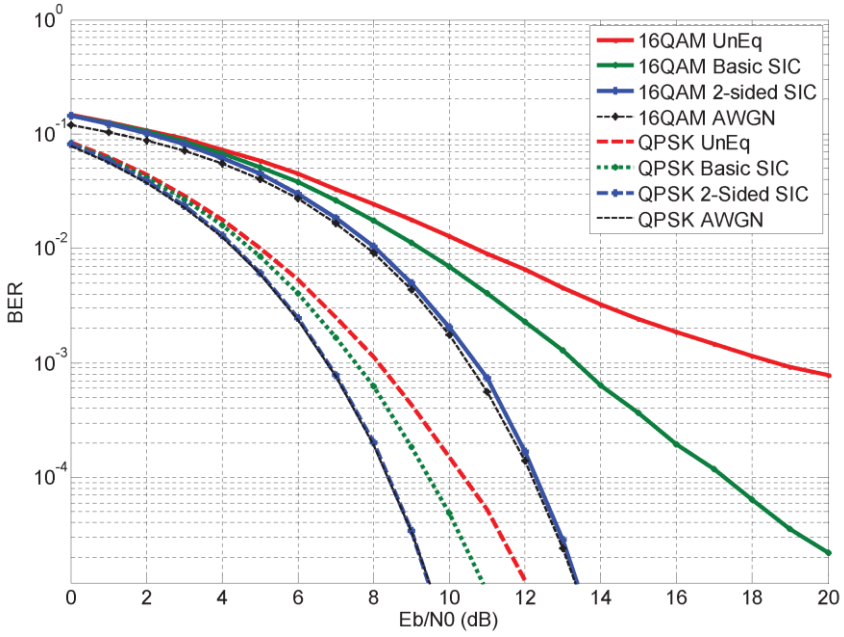

Figure 4-18: GFDM Double sided -SIC BER performance

4.3.3 CFO effects in GFDM

This subsection details the effect of CFO perturbation on GFDM bit error rate performance. The receiver and the transmitter system model are shown in Fig. 4-19 and Fig. 4-20, respectively.

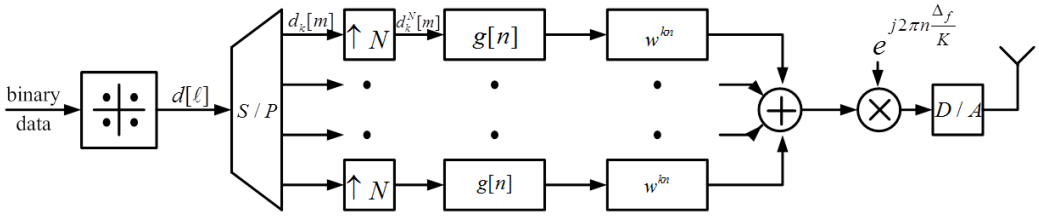

Figure 4-19: CFO-GFDM transmitter block

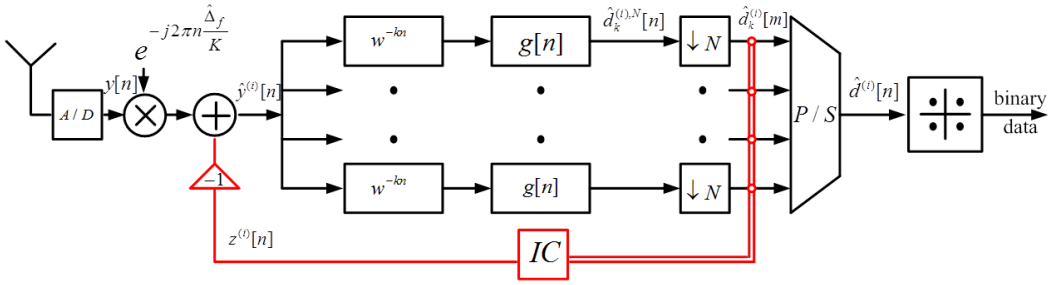

Figure 4-20: CFO–GFDM receiver block

The bit error rate performance of the CFO affected GFDM system shows that the perturbation is not that significant for CFO < 5% of the subcarrier bandwidth. For CFO higher than 5%, the BER performance is not good at all. The figure shows the BER performance of GFDM CFO affected, with or without ICI cancellation and then with estimated CFO cancellation.

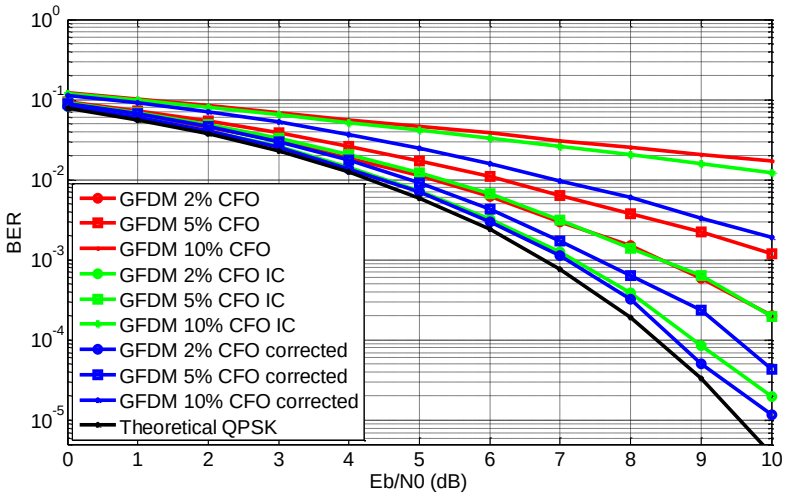

Figure 4-21: GFDM error rates in the presence of CFO

4.3.4 Sensing GFDM signals

An extensive work has already been done in sensing OFDM signals based on the energy detection principle, and in this subsection, we evaluate the sensing performance of GFDM signals. Other spectrum sensing techniques like cyclostationary feature based detection are more computationally intensive than simple energy detection and a comparison of these two methods is out of the scope of this work. Here we use a standard GFDM receiver for sensing an opportunistic signal. Whenever GFDM is used for CR TVWS transmission, it is convenient to use the GFDM receiver as a sensing device for other CR signals. Complementary ROC curves are obtained for sensing with a GFDM sensor and compared with ROC curves of an OFDM sensor.

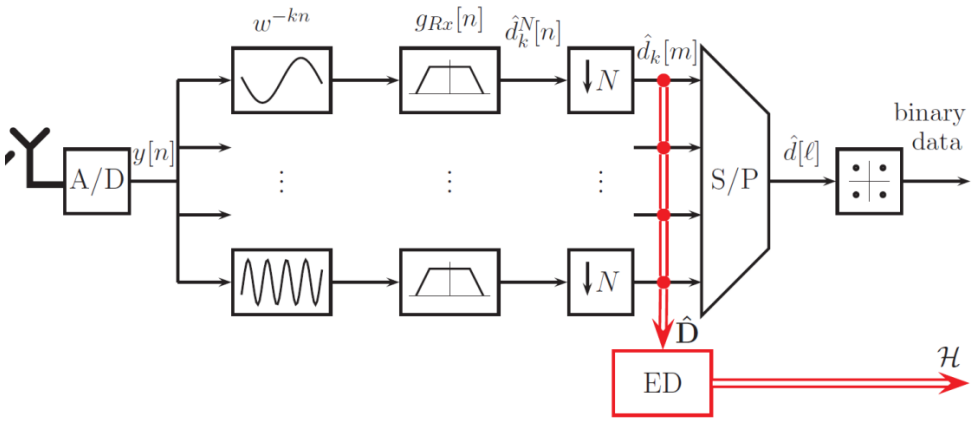

Figure 4-22: GFDM receiver system model for ED

The detailed block diagram of the energy detector is shown in Fig. 4-23. The GFDM receiver demodulates the received data and the data block D is passed through a square law device. The summer adds up the energy values of each of the samples along one subcarrier to compute the energy in each of the subcarrier bins. This sensing measurement is compared with a decision threshold to decide whether the subcarrier is empty or occupied. The vector H contains the decisions, either H0 or H1 for all the subcarriers in the CR system.

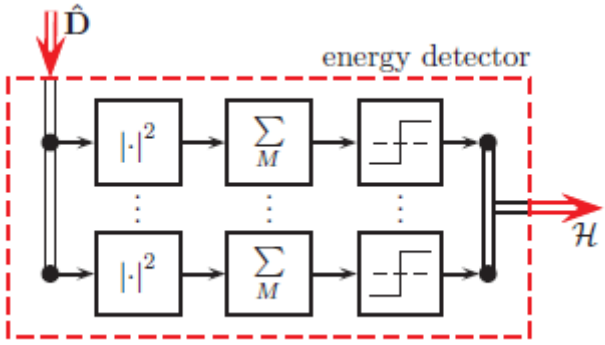

Figure 4-23: Energy detector block diagram

The scenario simulated here, is where the primary incumbent signals are protected with geo-location database query mechanism, but the opportunistic users in the TV white space need to be sensed before another signal can be transmitted in the same frequency band of operation.

Figure 4-24: Simulation setup of WS for opportunistic usage

The system is simulated with K = 128 subcarriers, where the TVWS is present in subcarriers K = 33 to K = 96, where the whitespace is in the center of the frequency band and 32 subcarriers on the left as well as on the right side carry opportunistic data. The adjacent subcarriers to the stop-band, i.e. the transition band, are not for transmission and hence are not considered in the calculation of the probability of false alarm and that of detection. The simulation parameters are tabulated in Table 1. Multipath channels and cyclic prefix were not considered in the setup.

4.3.4.1 Synchronous Receiver

Assuming perfect synchronization at the receiver, this system is simulated, once with OFDM and then with GFDM as cognitive opportunistic signals. The OFDM and GFDM systems are sensed with respective OFDM and GFDM sensors and ROC performance curves are obtained. The complementary ROC curves for GFDM match the complementary ROC curves for OFDM. These simulated curves follow the theoretical curves as shown in Fig. 4-25. This shows that the sensing performance with a GFDM sensor is comparable to ROC curves obtained from traditional OFDM sensors in synchronous systems. The SNR is varied from 0 dB to 4 dB in steps of 1 dB.

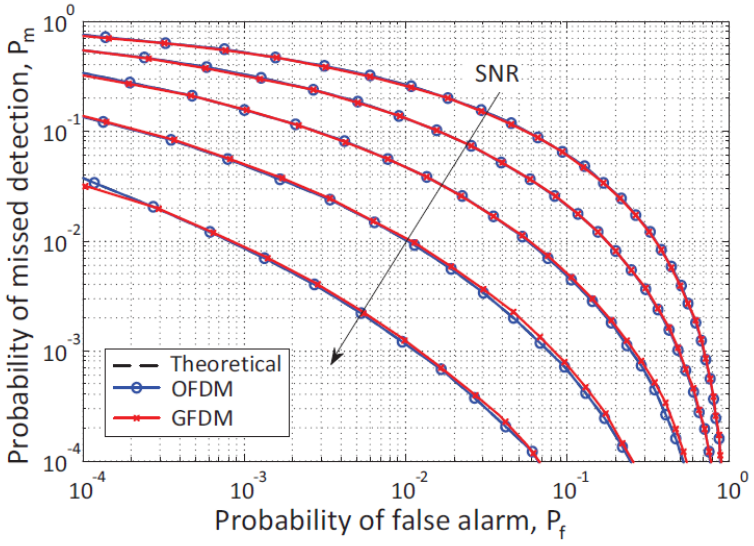

Figure 4-25: Complementary ROC curves for synchronous GFDM and OFDM with varying SNR

4.3.4.2 Asynchronous Receiver

A more realistic scenario is where we consider a frequency offset at the receiver. The worst case setup with an offset of half the subcarrier spacing is considered. The OFDM and GFDM signals are sensed by their respective OFDM and GFDM sensors and the complementary ROC is obtained. It is observed in Fig. 4-26, that the GFDM complementary ROC plots are better compared to OFDM ROC curves. Over the considered range of SNR and Pf , the probability of missed detection for an OFDM signal is higher than that of a GFDM signal. It is also observed that for higher values of SNR, the improvement

of the complementary GFDM ROC curves over OFDM ROC curves is larger. This implies that GFDM signals can be better detected as compared to an OFDM signal in asynchronous systems as OFDM is more prone to frequency offset. Hence GFDM sensing is more robust compared to OFDM sensing in more realistic scenarios. The SNR is varied from 0 dB to 4 dB in steps of 1 dB.

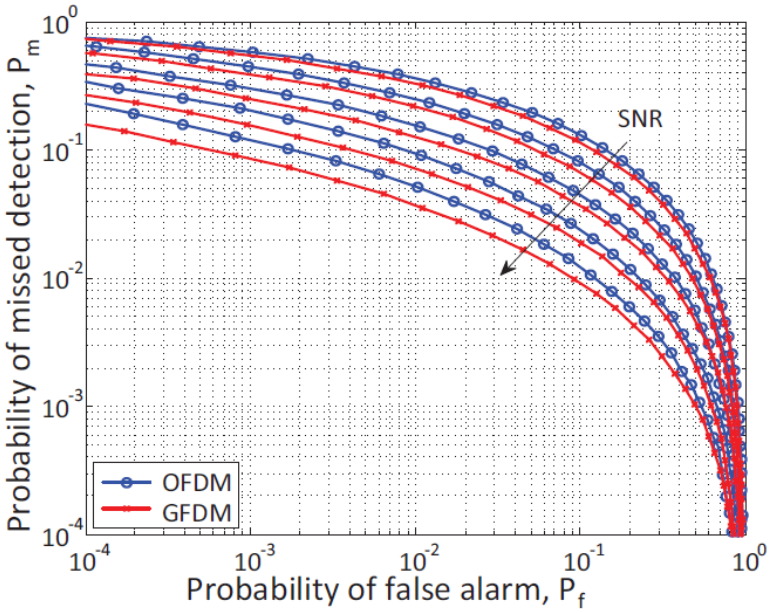

Figure 4-26: Complementary ROC curves for asynchronous GFDM and OFDM with varying SNR

4.3.4.3 Sensing with GFDM Receiver

In this simulation setup, we have considered an asynchronous CR system. All combinations of transmitting OFDM as well as GFDM and using an OFDM or GFDM receiver for sensing are considered. Based on this we have compared ROC curves for OFDM and GFDM receivers. These are known in Fig. 4-27. From the above figure, we see that the sensing ROC performance is best when a GFDM transmission is sensed by a GFDM receiver. The conventional ROC performance curves for OFDM sensing by a traditional OFDM based sensor is also shown here, and its performance is worse than that of the GFDM sensor. The most interesting observation from this study is that when OFDM transmission is sensed by GFDM sensor, then the ROC is better than that of an OFDM based sensor. The steep spectral shape of the GFDM filters improve the sensing performance of a OFDM opportunistic transmission. It is also clear from the above figure, that with higher SNR, sensing with GFDM receiver performance improves.

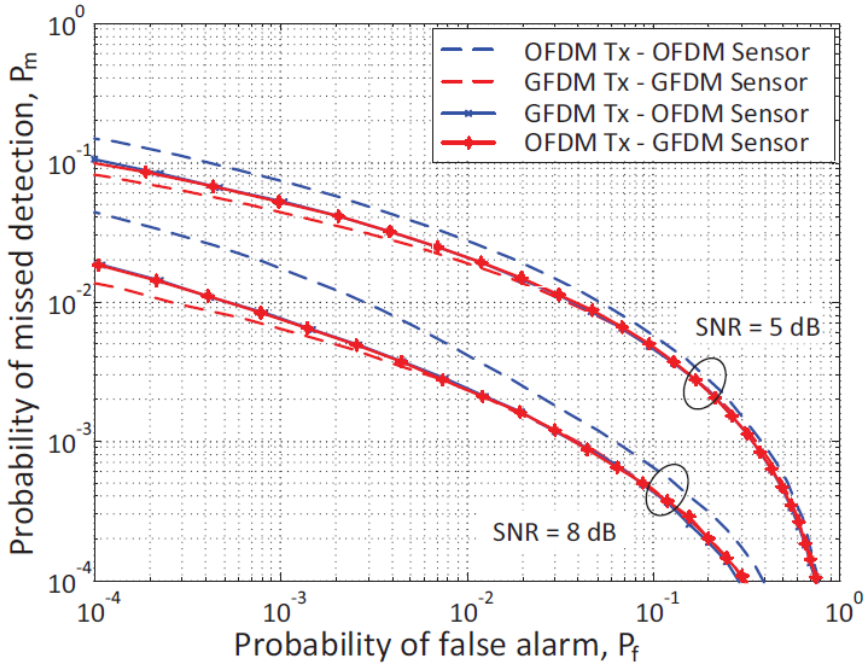

Figure 4-27: Complementary ROC for sensing with OFDM and GFDM receivers at SNR = 5 dB and 8 dB.

It is extremely important that the cognitive radio reliably detects not only incumbent active transmissions but also other opportunistic signals. GFDM is an extremely attractive multicarrier modulation scheme suitable for cognitive radio PHY as it has a low out-of-band radiation into the adjacent frequency bands. Traditional OFDM signal detection techniques and algorithms can be applied to GFDM as well. In this work, energy detection based spectrum sensing is simulated for the scenarios where OFDM and GFDM are used as opportunistic signals. It is observed that complementary ROC curves for GFDM are better than OFDM and GFDM can be better sensed than OFDM in an asynchronous cognitive radio system. It is also evident that using a GFDM receiver as a sensor also improves the ROC characteristics of a traditional OFDM system. These simulation studies show that compared to conventional OFDM, GFDM is more suitable for cognitive radio PHY, not only because of better spectral shaping, but also because of better sensing characteristics.

4.4 Conclusions

GFDM is a generalization of OFDM and it has a problem of self-ICI. The implementation of basic and double-sided serial interference cancellation for a GFDM multicarrier system has been done. It is shown that self-interference in GFDM is reduced by basic SIC and completely eliminated by double sided SIC. This section explains the GFDM concept and details the implementation procedure of the interference cancellation algorithms. In an extremely fragmented spectrum, like the recently made available TV white spaces, GFDM can be an attractive option as a physical layer modulation design for cognitive radio application. With its flexibility to choose the pulse shape, so that out-of-band leakage is minimum into the incumbent frequency band of operation, GFDM can be thought of as a next generation PHY design concept.

The research done in this section might have a potential impact on standardization activities. Lower ACLR achievements and improvement in sensing ROC curves might impact the standardization activities.

5 Advanced Multicarrier Technique: FBMC

This section presents a rather novel modulation schemes that QoSMOS considers for TVWS physical layer operation. While in the previous chapter OFDM-derivatives have been proposed that either feature quick adjacent channel roll-off or can produce deep notches in the transmission band, the schemes in the present chapter are designed specifically by considering general multicarrier modulation, and the scheme exhibit extremely low levels of adjacent-channel leakage under ideal conditions. Various sorts of FBMC schemes are rather mature with practical applications in wired and wireless systems.

In this chapter we briefly describe the concrete FBMC scheme proposed for the QoSMOS implementations, OFDM/offset QAM. Then some novel practical algorithms and link-level investigations are presented that will eventually lead us to a working link-level specification and also give some guidelines for the practical proof-of-concept implementation. We consider among others synchronization, equalization and PAPR aspects.

We also briefly introduce the recently invented GFDM scheme, and give new simulation results on its link-level performance with different interference cancellation schemes. Also preliminary synchronization results are given. Finally, the two generalized schemes are compared.

5.1 Description

FBMC has been considered in QoSMOS, and special focus has been put on OFDM/OQAM based FBMC. As presented in [D4.1], FBMC techniques may be divided into 3 families of multicarrier modulations techniques: Filtered multitone (FMT), Cosine modulated multitone (CMT) and staggered modulated multitone (SMT) or more commonly multicarrier with offset QAM (OFDM/OQAM). Since the FMT method does not achieve maximum bandwidth efficiency, this option has been discarded from our study. And as already mentioned in [D4.1], it was shown in [Farhang-Boroujeny2010] that CMT and OFDM/OQAM are closely related through a modulation step and a one-to-one mapping of data symbols. The core of the FBMC system is the transmultiplexer (TMUX) configuration shown in Figure 5-1. The main processing blocs in this direct form representation are OQAM-preprocessing, synthesis filter bank, analysis filter bank, and OQAM post-processing.

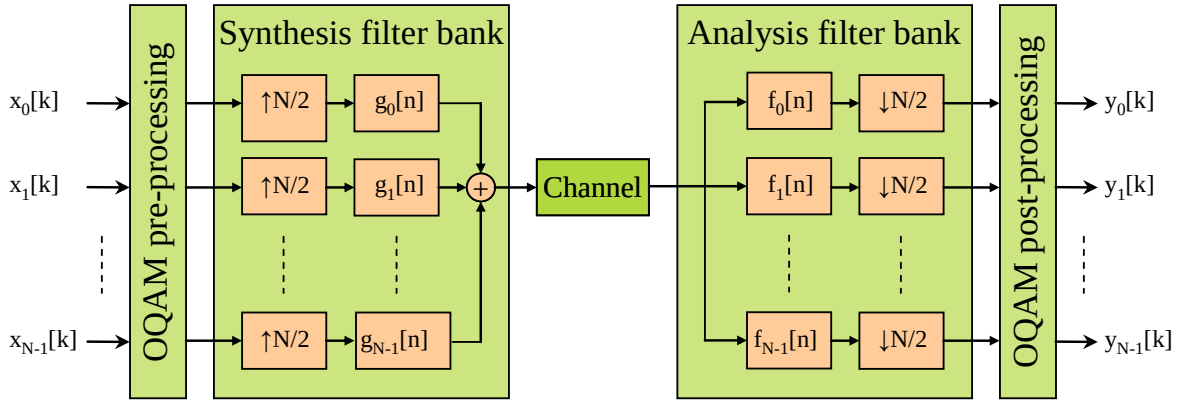

Figure 5-1: FBMC transceiver architecture (Direct Implementation)

Data at the input of the modulator is pre-processed using OQAM. It consists of a complex-to-real domain conversion of the QAM baseband signal, as shown in Figure 5-2. The complex-to-real conversion forms new symbols, $d_{k,2l}$ and $d_{k,2l+1}$. The complex-to-real conversion increases the sample rate by a factor of 2. The real and imaginary part of the QAM are interleaved in time and frequency

and multiplied by the $\theta_{k,n}$ sequence, where k is a carrier index and n a time index. Various sequences of $\theta_{k,n}$ are possible to guarantee orthogonality at the transmitter of the OFDM/OQAM symbols. The sequence chosen by QoSMOS is the following:

$$\theta_{k,n} = j^{(n+k)} \tag{5-1}$$

where $(j)^2 = -1$.

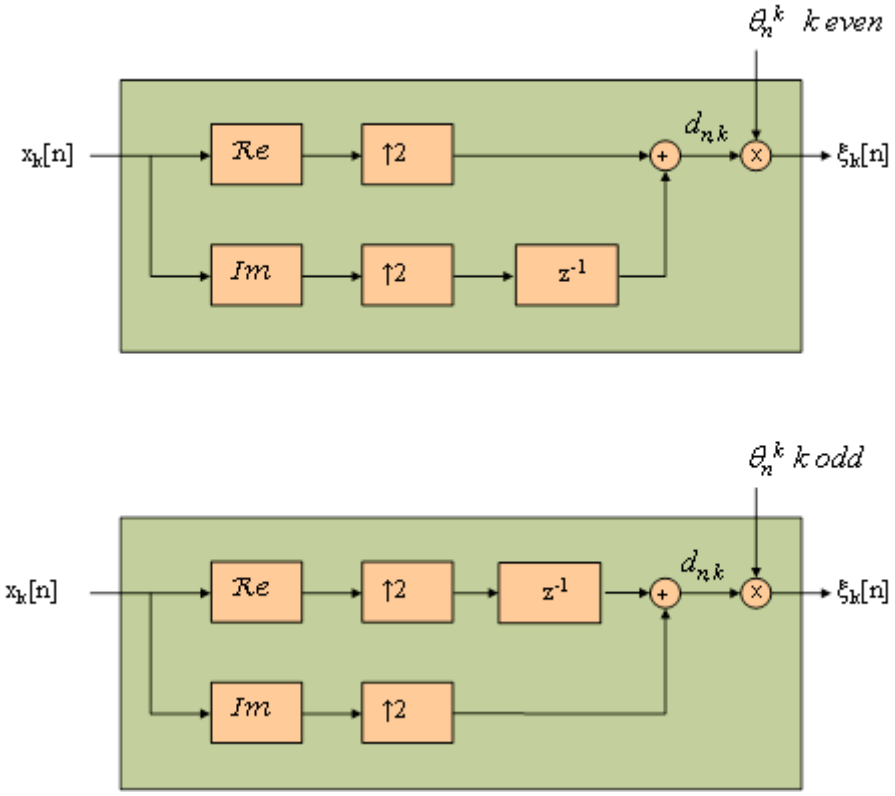

Figure 5-2: Example of OQAM preprocessing
(a) k even, (b) k, odd, where k is the carrier number

The OQAM-postprocessing block converts the received filtered and decimated OQAM symbols into estimated QAM soft inputs. It consists of two operations that are dual to the preprocessing process: the first operation is the multiplication by $\theta_{k,n}^*$ sequence (where * is the complex conjugate transform) and a real-to-complex conversion.

Filterbank synthesis consists on N oversamplers followed by N filters. Signals at the input of the filterbank are indeed first oversampled by a factor of $N/2$, and then filtered by the impulse response of $g_k[n]$, the k^{th} filter and is defined by:

$$g_k[n] = g[n] \cdot \exp\left(j \frac{2\pi k}{N} \left(n - \frac{L_p - 1}{2} \right) \right) \tag{5-2}$$

where $g[n]$ is a low pass filter called the prototype filter, and is of duration L_p. It is common practice to impose that L_p is a multiple or almost a multiple of N ($L_p = KN$, $L_p = KN-1$, $L_p = KN+1$ are possible choices).

Synthesis and respectively analysis filter may be implemented with an IFFT followed by a polyphase network structure or a polyphase network followed by an FFT respectively [Hirosaki1981, Siohan2002]. This implementation makes FBMC architecture similar to OFDM and justifies the denomination of OFDM/OQAM (see Figure 5-3).

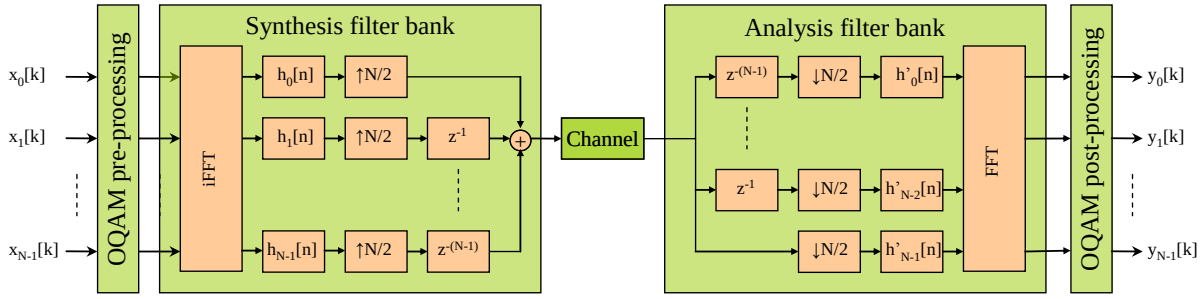

Figure 5-3: FBMC transceiver architecture (PPN and FFT implementation)

The prototype filter of FBMC has a direct consequence on the way burst packet transmissions should be synchronized. Let's suppose that N_b blocs of N QAM-FBMC symbols are transmitted (at the input of the OQAM-preprocessing block). The signal at the output of the synthesis filter bank starts with a rise time of duration $(L_p-1)/2$ (or $(K-1)/2$ blocks of N-complex symbols) and is followed by a steady state period where the transmitted symbols are output and finishes with a fall time of duration $(L_p-1)/2$. An example of burst is given in Figure 5-4.

The filter bank allows for the control of the frequency response of the transmitted signal. This is illustrated in Figure 5-5. A prototype filter that spans over *4* OFDM symbols ($K=4$), meets the out-of-band rejections requirement set in Section 3.2, for both FCC and OFCOM. While OFDM requires an external transmit filter to meet the requirement, the built-in filter of the FBMC allows out-of-band rejection that is significantly below 55 dB of rejection.

The PAPR properties of FBMC are very similar to those of OFDM. The complementary cumulative distribution functions (CCDF) of FBMC and OFDM are compared on Figure 5-6 for the proposed 15 kHz subcarrier spacing (481 subcarriers) and for possible smaller subcarrier spacing, resulting in 964 subcarriers over the same bandwidth. Hence, system designers face the same issue with the peak power, and appropriate measures need to be taken to prevent spectrum re-growth resulting from nonlinear distortion caused by e.g. power amplifiers.

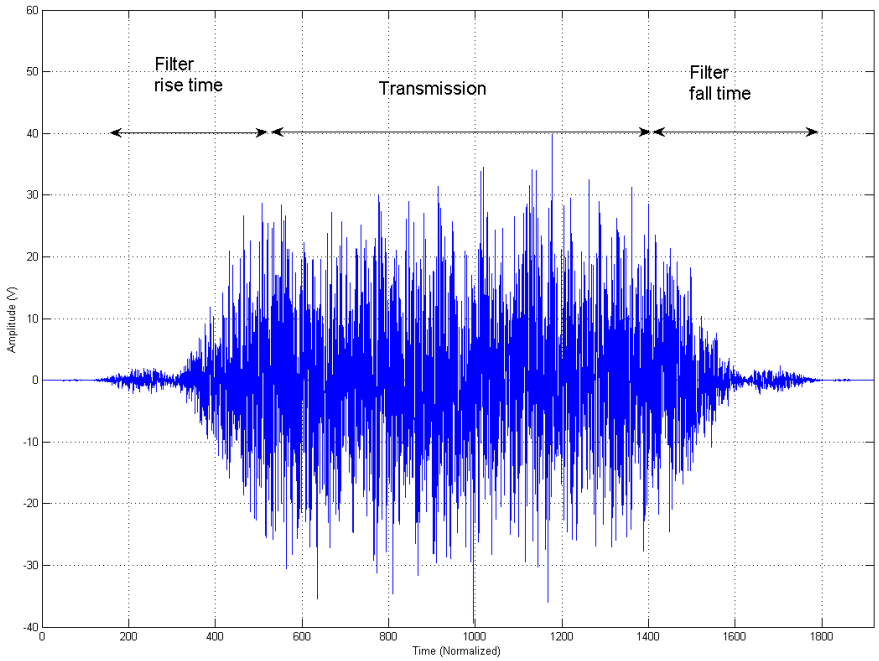

Figure 5-4: Example of FBMC packet – real part of signal, *K=4, N=256*.

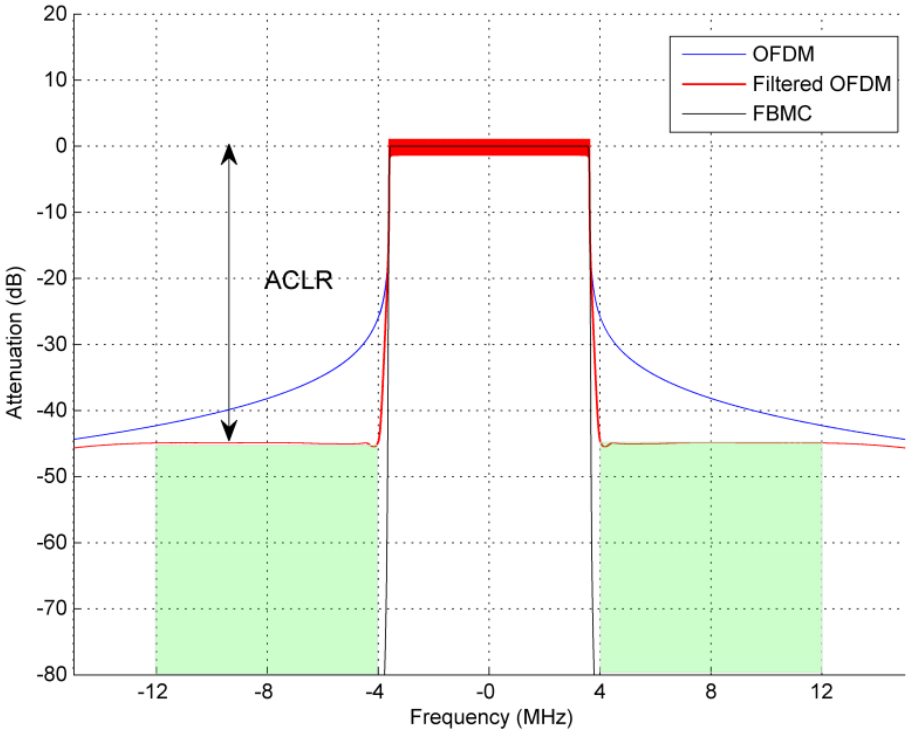

Figure 5-5: Power Spectral Density: OFDM vs. FBMC

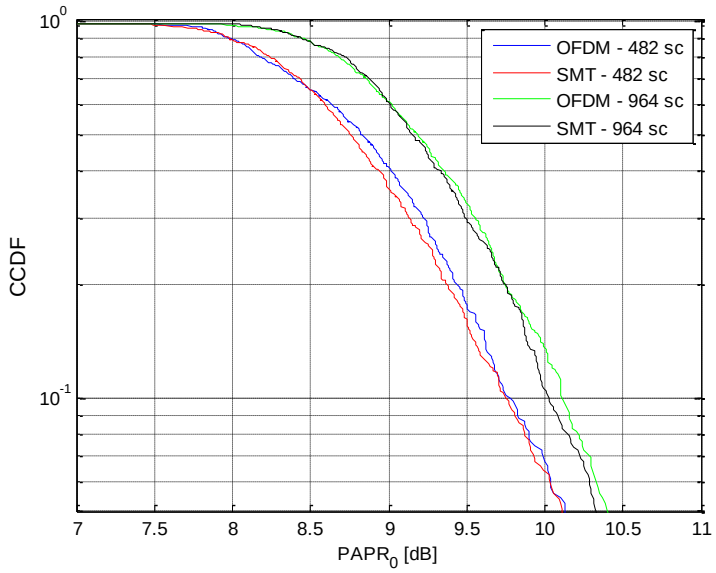

Figure 5-6: PAPR comparison of OFDM and FBMC

5.2 Synchronization

5.2.1 Symbol synchronization

Symbol and frequency synchronization is usually performed by introducing a preamble before the block of data. For classical CP-OFDM, a repetitive sequence of shorter duration is often introduced [Fort2003]. This sequence is repeated and synchronization may be performed by autocorrelation. The data symbols directly follow the preamble. This cannot be the case in FBMC, as data symbols would interfere with the preamble and increase significantly synchronization estimation errors. Instead, it is suggested to send a known periodic preamble and to leave a gap between the preamble and the data symbol to avoid any interference from the data symbols to the preamble.

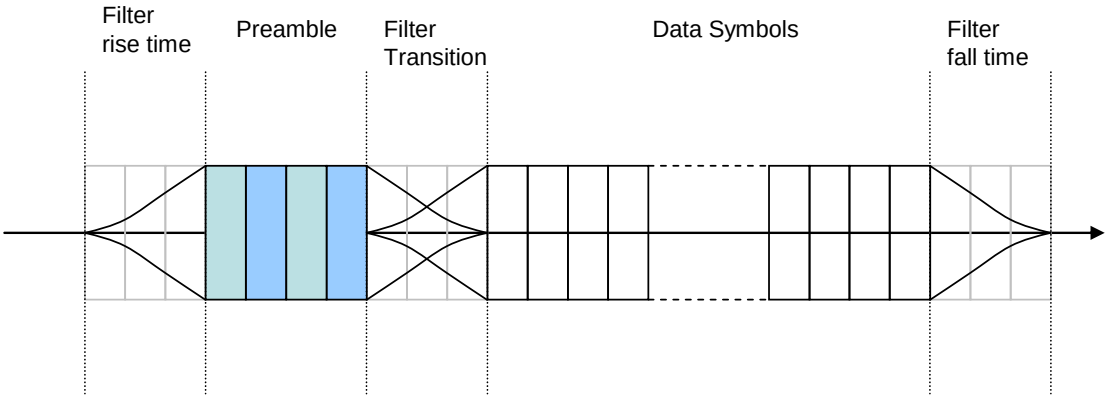

Figure 5-7: Structure of synchronization preamble.

Fusco et al. [Fusco2009, Petrella2009] proposed a symbol and frequency synchronization based on the same structure of preamble. It is inspired by the fundamentals used in OFDM and summarized in [Morelli2007]. It consists on emitting a training sequence with the following property:

$$s_{TR}(k+N) = s_{TR}(k) \tag{5-3}$$

where s_{TR} is the repeated transmitted sequence. Many estimators have been proposed and are based on the estimated time autocorrelation:

$$R(\tilde{\tau}) = \sum_{k=0}^{(P-1)N} r^*(k+\tilde{\tau}) \cdot r(k+N+\tilde{\tau}) \quad (5\text{-}4)$$

where r is the received signal after sampling the transmitted FBMC symbols through a noisy transmission channel, P is the duration of the training sequence in blocks of N symbols (or FBMC symbol). The maximum of amplitude of $R(\tau)$, corresponds to the detection of the optimum symbol. Its phase is used to estimate the frequency error between the transmitter and the receiver.

A refinement of the technique consists on adding the inter-correlation of the emitted sequence to the estimation process in order to reject the impact of the noise.

$$S(\tilde{\tau}) = \sum_{k=0}^{(P-1)N} r^*(k+\tilde{\tau}) \cdot s_{TR}(k) \cdot r(k+N+\tilde{\tau}) \cdot s_{TR}^*(k+N) \quad (5\text{-}5)$$

Both techniques are implemented in the time domain.

Although s_{TR} may be generated independently from the synthesis filter, the algorithms are evaluated using a sequence that is generated through the synthesis filter. A necessary condition for (6-3) to be valid is to have the same condition at the input of the synthesis filter bank, or the QAM sequence follows the following condition:

$$x_{TR,k}(n+1) = -x_{TR,k}(n) \quad (5\text{-}6)$$

for the duration of the training sequence. This is because of the chosen $\theta_{k,n}$ sequence and $(j)^2=-1$.

The estimator proposed in (6-4) presents the advantage of being blind and simple to implement. However, the variance of its symbol synchronization estimate may be quite large. This is the case for OFDM and even more so for FBMC as the correlation usually presenting a triangle shape gets smoothed by the prototype filter in the case of FBMC. An example of the shape of the autocorrelation is given in Figure 5-8 for 64 carriers and a preamble of duration of 4 FBMC symbols (64x4 samples).

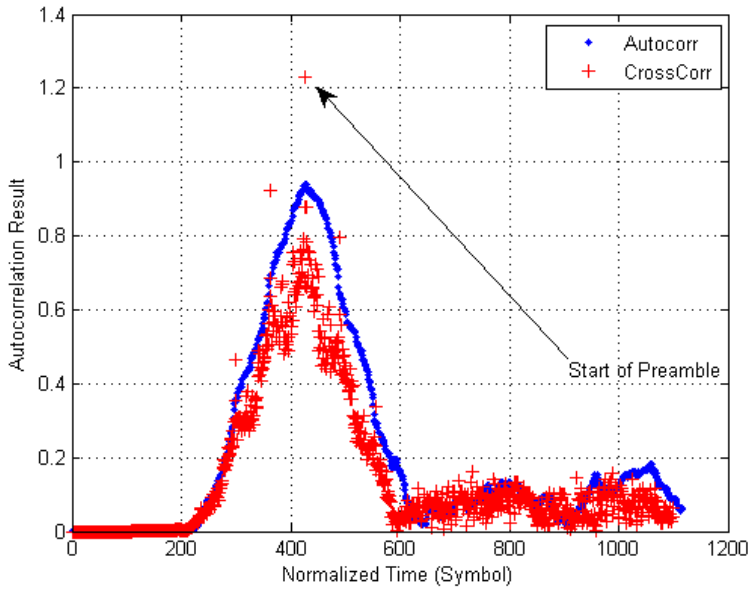

Figure 5-8: Example of preamble autocorrelation and cross-correlation algorithms (*N=64, Repetition of preamble 4*).

The shape of the cross-correlation is also given for a perfect channel without any noise.

For the autocorrelation algorithm, although the start of the preamble is detected reliably, the exact position of the first symbol of the frame is much more difficult to detect, this explains why, even under relatively high carrier-to-noise ratio, the variance of the symbol synchronization algorithm based on (6-4) is expected to be large. For the case of the cross-correlation algorithm of (6-5), the exact start of the FBMC symbol may be found with a much lower variance, but the cost of implementation is extremely high when the number of carrier is large as a cross-correlation of size duration of the preamble should be estimated for every received sample.

We therefore suggest the use of a new synchronization algorithm and propose to evaluate this newly developed algorithm against the autocorrelation algorithm of (6-4). We propose to estimate an alternative cross-correlation after the analysis filter bank but before the OQAM-postprocessing. If the preamble sequence is such that it fulfils (6-6), then the data at the input of the synthesis filter bank is constant. Since the prototype filters are lowpass filters, the received sequence is also constant and is the superposition of the data sent at time $2n$, which is real data (respectively pure imaginary data) on even (respectively odd) carrier numbers and the data sent at times $2n+1$, which is pure imaginary data (respectively real data) on even (respectively odd) carrier numbers. Therefore, if the frequency error is bounded to a level that is small in comparison to the carrier spacing, the received sequence, at the output of the synthesis filter and on carrier q, may be expressed as:

$$y_{q,n} \approx e^{j\left(2\pi\frac{\varepsilon}{2}+\phi\right)} \cdot e^{-j\frac{2\pi q\tau}{T}} \left(d_q^{\mathrm{Re}} + jd_q^{\mathrm{Im}}\right) H_q + \eta_{q,n} \qquad (5\text{-}7)$$

where d_q^{Re} and d_q^{Im} are function of the transmitted preamble sequence and H_q is the channel frequency response on carrier q, ε is the normalized frequency error and τ, the symbol time offset and $\eta_{q,n}$, an additive noise term.

We therefore propose to estimate the symbol synchronisation, in the frequency domain, by cross-correlation of the output of the analysis filter by the a priori expected sequence of $(d_q^{Re} + jd_q^{Im})^*$. The symbol synchronization error may then be estimated by applying an inverse FFT to the result and locate the peak of the channel amplitude. Because of the effect of the cross-correlation in the frequency domain (effectively a circular cross-correlation), an uncertainty should be removed in the symbol synchronisation. One way to remove the uncertainty is to associate both synchronization schemes and use the autocorrelation technique for coarse symbol and frequency synchronisation, while the proposed frequency domain cross-correlation algorithm may be used for a fine synchronisation.

The variance of the algorithm is estimated and compared to algorithms (6-4) and (6-5) for Additive white Gaussian channels and Multipath channels (ITU-R Pedestrian A channels, at 3 km/h). The results are shown in Figure 5-9.

The frequency domain synchronization algorithm outperforms the autocorrelation and the cross-correlation algorithms. Since the algorithm may be efficiently implemented using the FFT, it is usually more cost effective than the time domain cross-correlation algorithm. The autocorrelation algorithm however, presents the advantages of being simple to implement and give a reliable frequency error estimate.

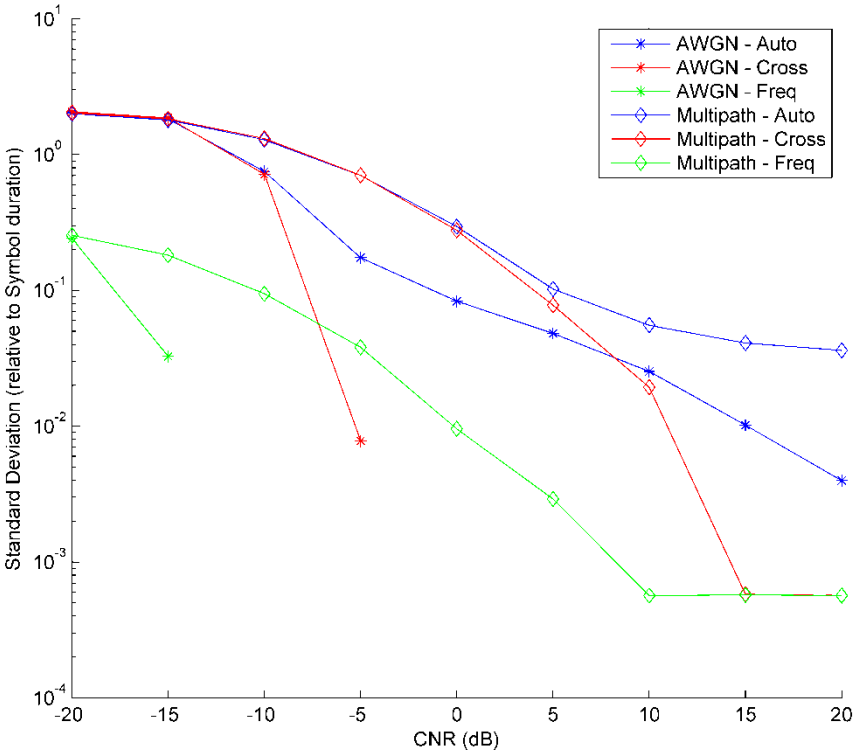

Figure 5-9: Performance result of synchronization algorithms. (Number of Carriers is 1024, Preamble duration is 4 OFDM symbols).

5.2.2 Carrier synchronization

A well-known drawback of OFDM is its sensitivity to frequency inaccuracy which causes loss of orthogonality among neighbouring subcarriers and hence leads to performance degradation. In order to compare FMBC/SMT with conventional OFDM regarding their sensitivity to Carrier Frequency Offset (CFO) and phase noise, simulations have been performed [Kollár2011b]. As a representative result, Figure 5-10 shows bit error rates for uncoded 16QAM modulation, assuming perfect synchronization and a CFO of 0.03 subcarrier spacing, respectively. Clearly, FBMC has similar sensitivity to this impairment. The offset between the curves, which is attributed to the SNR gain due to the lack of cyclic prefix in the case of FBMC/SMT, remains the same regardless of the presence of CFO.

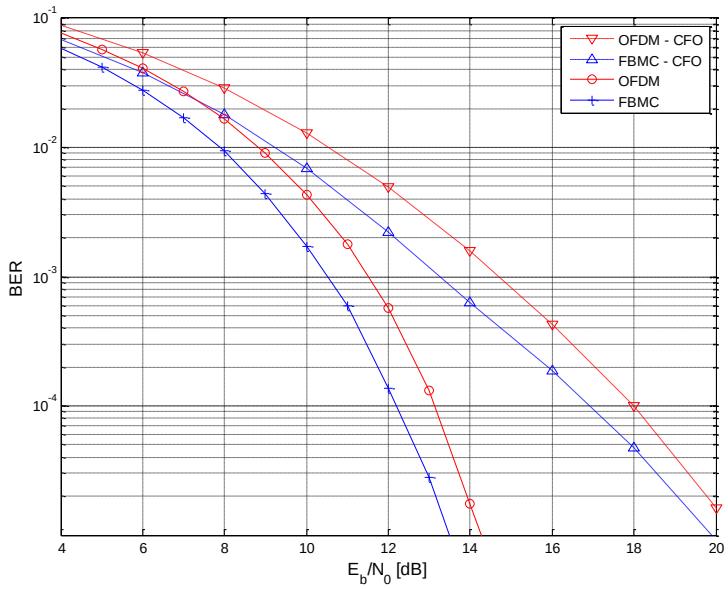

Figure 5-10: CFO sensitivity of FBMC/SMT and OFDM

Similar findings apply to the impairments caused by the presence of phase noise in the oscillators. As seen in Figure 5-11, where again 16QAM modulation is used, the same offset remains between OFDM and FBMC/SMT when a Gaussian phase noise with 8 degrees standard deviation is assumed instead of ideal components in the transmitter chain.

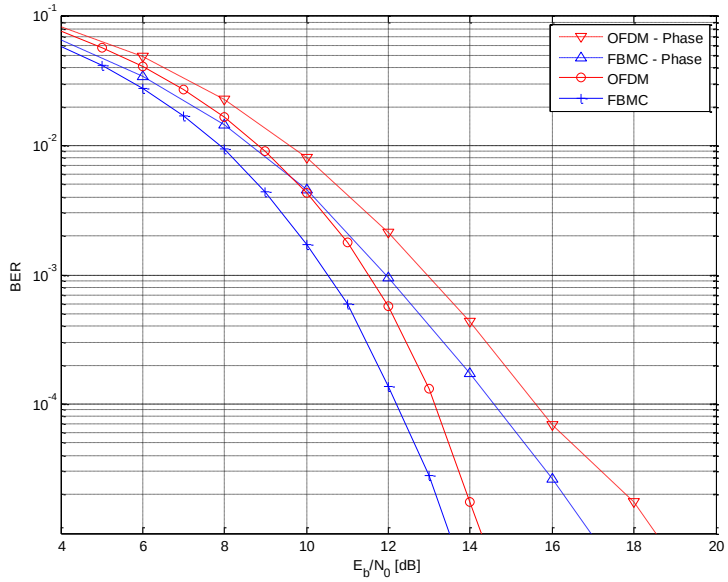

Figure 5-11: Sensitivity of FBMC/SMT to phase noise

Consequently, when frequency/phase synchronization is considered in a practical situation, one can resort to similar performance requirements that are considered for conventional OFDM transmission.

5.3 Link-level performance

After synchronization of the received signal, the next step is to perform channel equalization. In FBMC systems the channel equalization procedure is not as straightforward as it is in OFDM due to the absence of the cyclic prefix. For OFDM systems, as long as the channel time dispersion is shorter than the CP, linear channel equalization can be performed in the frequency domain without any deteriorating effect caused by inter-symbol-interference (ISI). In FBMC systems the symbols are longer than in OFDM: as a result the ISI for multipath channels with small delay spreads are almost negligible, and a low complexity per-subcarrier equalizer called AP-ASCET [Ihalainen2002] can be utilized to perform channel equalization. Each subcarrier is equalized using a single complex channel gain. The simplest approach is the ZF, where the received complex symbol is divided by the complex channel gain:

$$X_k^{ZF} = \frac{Y_k}{H_k} \tag{5-8}$$

The Minimum Mean Squared Error (MMSE) technique gives a better result, due to the fact that it takes also the noise power N_0 and the signal energy E_s into account. The compensation value can be expressed as

$$C_k = \frac{1}{H_k^{MMSE}} = \frac{H_k^*}{|H_k|^2 + \frac{N_0}{E_s}} \tag{5-9}$$

Dealing with channels with longer delay spreads, other equalization techniques need to be considered for FBMC such as those presented in [Kollár2011a], otherwise error floor will appear even at high SNR values.

For the FBMC system the well-known MMSE criteria has to be modified to include the power of the ISI. The modified compensation coefficient for the incoming symbols can be calculated as

$$\frac{1}{H_k^{MMSE}} = \frac{H_k^*}{|H_k|^2 + \frac{N_0 + I}{E_s - I}} \tag{5-10}$$

To further improve performance of the MMSE technique for FMBC, we propose using time diversity averaging. The averaged MMSE is driven by the idea that the ISI can be also considered as a noise, which can be eliminated by averaging. Based on the idea of moving the observation window, we perform the demodulation and MMSE equalization for each of the Δn positions of the possible L observation windows and then we average all complex modulation values belonging to the same subband:

$$X_k^{AVG} = \frac{1}{L}\sum_{\Delta n=0}^{L-1} X_k^{MMSE}(\Delta n) = \frac{1}{L}\sum_{\Delta n=0}^{L-1} \frac{Y_k(\Delta n)}{H_k^{MMSE}(\Delta n)} \tag{5-11}$$

The link-level performance curves are shown for the IEEE 802.22 WRAN channels. This choice is motivated by the fact that channels with long temporal dispersion are challenging from the equalization point of view. Therefore it is important to demonstrate that FBMC can cope with these equalization requirements, and the computational complexity is still reasonable when compared to the very simple equalization requirements of conventional OFDM-based systems.

Table 5-1 summarizes the physical layer parameters for the link-level performance simulations. The same generic parameters are employed that have been devised in Chapter 3. A relatively simple and rather weak convolutional FEC code will be assumed. This choice is consistent with the initial plans for the proof-of-concept implementations.

Table 5-1: Simulation parameters for FBMC transmission performance

N – number of subcarriers	1024
Nu – Number of used subcarriers	482
CP (only for OFDM)	256
K (only for FBMC)	4
Subcarrier spacing	15 kHz
Modulation	16-QAM
Coding	Convolutional coding (6,7) rate ½ with interleaving

The BER simulation results over 802.22 Channel profile B and C can be seen in Figure 5-12 and Figure 5-13, respectively. The previously mentioned problems can be observed. Especially in Channel C where the delay spread is much larger, FBMC has an error floor with all of the proposed equalizers. It can be also observed that FBMC has a comparable BER to OFDM, and with additional error correction codes, the BER can be pushed under a required threshold.

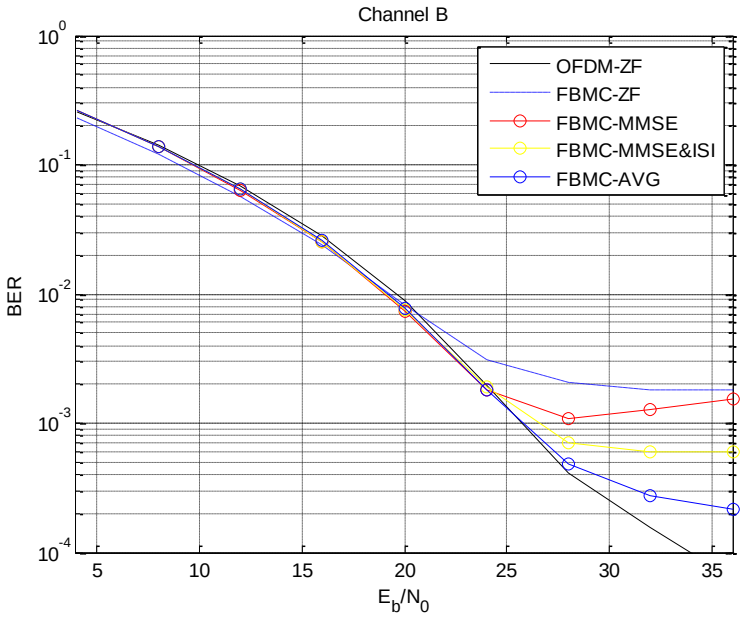

Figure 5-12: BER performance of FBMC over 802.22 Channel B

It can be seen in the BER simulations for Channel B, that until the CP is long enough to prevent ISI, OFDM can outperform FBMC above a certain SNR value. It can be also observed that the original equalization technique using ZF forcing can be further improved when taking the ISI into account and using a time diversity combining averaging technique.

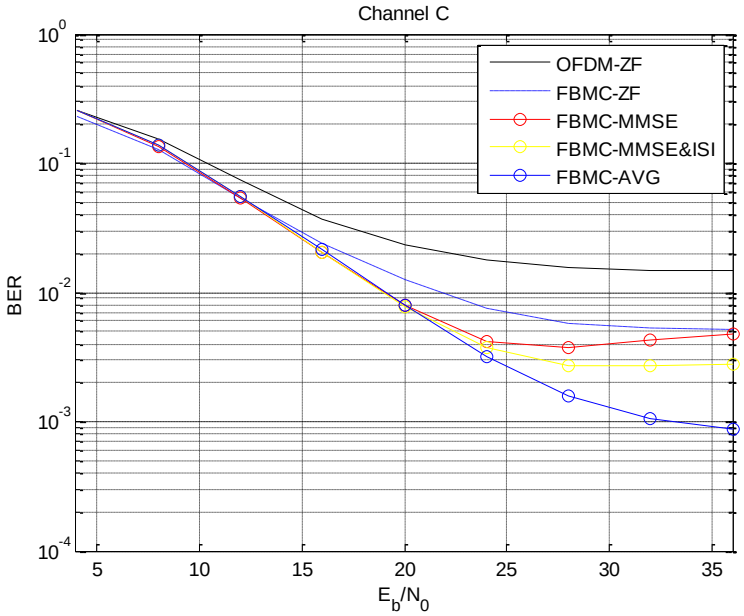

Figure 5-13: BER performance of FBMC over 802.22 Channel C

In the BER simulations for Channel C FBMC outperforms OFDM, due to the fact that the CP is not long enough to prevent ISI caused by the multipath propagation channel. A similar result can be observed for the proposed equalization schemes for FBMC. The best performance is provided by equalization using time diversity averaging.

Applying a novel iterative equalization technique [Kollár2011], the BER can be further improved. The results can be seen in Figure 5-13. In order to suppress the previously shown error floors in the BER, an iterative decision feedback scheme was presented [Kollár2011a]. The block diagram of the proposed scheme is shown in Figure 5-14.

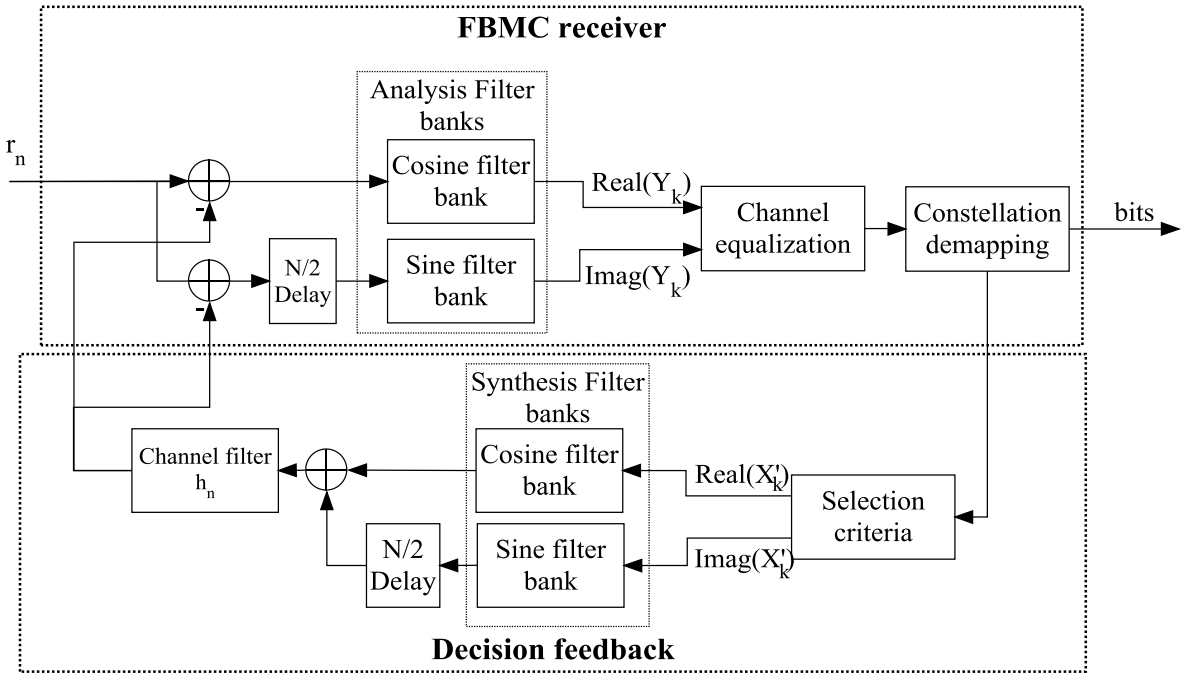

Figure 5-14: Block diagram of the decision feedback equalization scheme

The basic idea of the presented iterative receiver is to re-modulate some of the received modulation symbols and remove the effects the channel filtered signal components which may cause ISI before performing demodulation. If a decision is performed for the shaded *i*th FBMC symbol in Figure 5-15 of the cosine filter bank, then the receiver tries to reconstruct as much as possible from the surrounding symbols *i*-3, *i*-2...*i*+3 which overlap with it (both sine and cosine) based on the selection criteria. Then, during the decision on the *i*th FBMC symbol the ISI of the known neighboring symbols can be subtracted, reducing the noise stemming from the ISI, leading to better performance. The selection criteria is defined based on the constellation diagram, we take confidence interval around each constellation point. The complex modulation symbols which fall inside this interval are considered as reliable. During the iteration process the interval can be enlarged as the ISI is minimized.

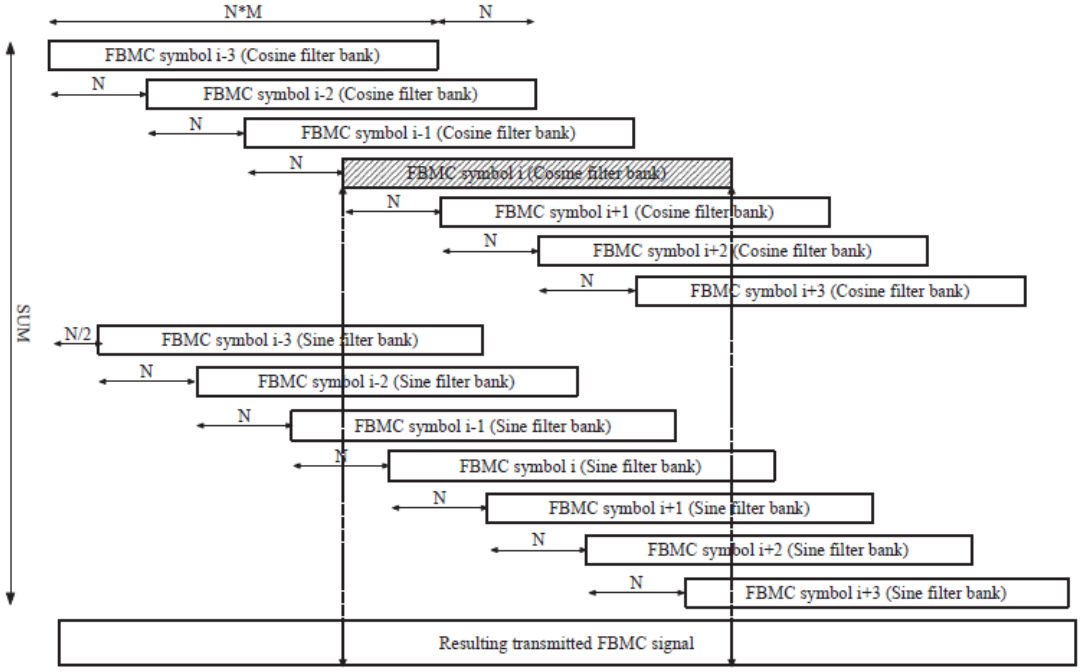

Figure 5-15: Generation of an FBMC symbol with an overlapping factor of 4

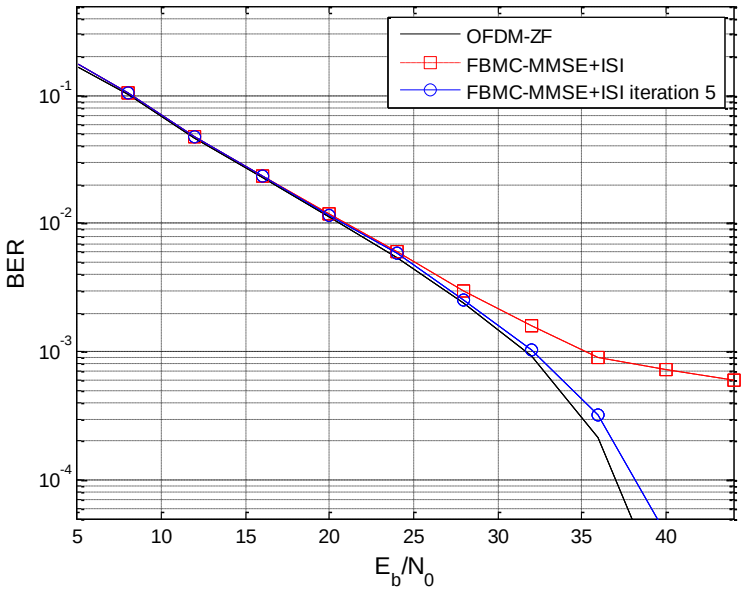

Figure 5-16: BER results of the iterative receiver compared to the conventional FBMC receiver over 802.22 Channel B

The BER results for coded FBMC using the proposed iterative equalizer are shown in Figure 5-16. It can be seen that the error floor can be further suppressed with only a few iterations. OFDM still slightly outperforms FBMC, but the performance was significantly improved and for practical purposes the difference is negligible.

This technique is similar to turbo equalization, but it only applies hard decisions. As a conclusion it is assumed that the performance can be further improved using soft decision based receiver taking

advantage of the turbo principle. The application of Turbo coding in FBMC scheme is being further researched. Turbo codes require soft demapping/decoding of the signal. In OFDM systems, as long as the CP is sufficiently long, Maximum Likelihood detection is possible. However, soft demapping/decoding in FMBC is not straightforward due to the presence of ISI. The effects of ISI have to be also considered during the soft demapping procedure.

5.4 Implementation aspects

5.4.1.1 Pilot scheme selection for channel estimation and synchronization

The simplest approach for pilot scheme construction is given by Javaudin et al. [Javaudin2003]. They propose an OFDM-like scheme where the pilots are scattered in quincunx (a geometric pattern consisting of five points arranged in a cross). The channel estimation is performed using interpolation in time and frequency domain using two methods: Wiener filtering and prolate sequences.

Compared to OFDM, the main problem of FBMC is the adverse influence of inter-carrier interference (ICI) and inter-symbol interference (ISI) stemming from the neighbouring subchannels/symbols, which also affect the pilot symbols and affect the performance of channel estimation and synchronization. This motivates the search for more suitable piloting schemes specifically designed for FBMC systems. In [Bader2010] and [Bader2011] the authors aim to design a WiMAX compatible waveform based on FBMC. They propose a modified pilot pattern for MIMO application, where auxiliary pilot carriers are applied which are designed to minimize interference effects on the pilots. Auxiliary pilots (also called “help pilots”) are positioned adjacently to the pilots position with the same modulation and they are used to minimize the interference effect caused by the multipath channel. Based on the same basic structure, [Yoon2008] introduces a more advanced pilot structure (a so called two-dimensional pilot block) for FBMC systems using IOTA filters, with better performance.

Ref. [Kang2007] suggests for FBMC systems applying Isotropic Orthogonal Transform Algorithm (IOTA) filters to use a preamble-based channel estimation scheme instead of a pilot-based one.

In the latest work of Stitz et al. [Stitz2010], a detailed analysis is given on pilot-based synchronization and equalization. They suggest a WiMAX-like pilot scheme with auxiliary pilots similar to the scheme proposed in [Bader2010], but with small modifications regarding the positioning of the pilots.

The best compromise between data rate loss and quality of channel estimation seems to be the block-based approach with pilots surrounded by auxiliary carriers. This scheme is illustrated in

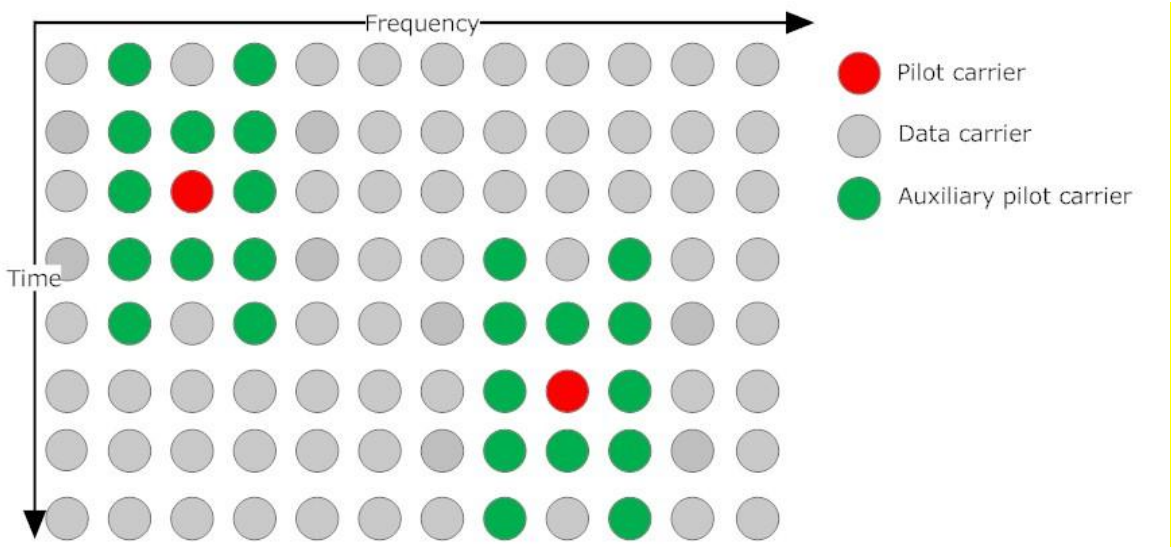

Figure 5-17: Scattered FBMC pilot scheme with auxiliary pilots [Yoon2008]

5.5 PAPR reduction techniques for FBMC

In this subsection, we propose and compare various methods to reduce the peak-to-average power ratio. A novel turbo-based iterative scheme is presented first, then Tone Reservation (TR) and Active Constellation Extension (ACE) is also presented. To our best knowledge, application of the latter two schemes to FBMC is also novel.

When dealing with multicarrier schemes, a critical problem is the large dynamic range of the signal. The peak-to-average power ratio (PAPR) is one of the measures used to characterize this dynamics, which is defined as:

$$PAPR(s(t)) = 10\log_{10}\left(\frac{\max\{|s(t)|^2\}}{E_s}\right) \quad (5\text{-}12)$$

where $|s(t)|$ is the amplitude of the transmission signal and E_s is the average energy of the signal. Both SMT and OFDM signals have large PAPR. Many techniques have been proposed for reducing the PAPR of OFDM [Lee2005]:

- amplitude clipping and filtering
- coding, interleaving
- partial transmit sequence (PTS)
- selective mapping (SLM)
- tone reservation
- tone injection (TI)
- active constellation extension

Each method has its own advantages and disadvantages. Clipping introduces distortion, which is in general not acceptable for TVWS communications where strict ACLR requirements are present. Some methods need increased power, others cause data rate loss and in some cases additional information is needed for the receiver. Most of the techniques are not applicable to FBMC/SMT due to the fact that the time domain symbols overlap (unlike in OFDM, where each symbol can be treated separately). Some solutions can be found in the literature for SMT such as clipping [Rahim2009] and overlapped SLM technique [Skrzypczak2006]. Most of these techniques (coding, interleaving, PTS, SLM, TI) are not directly applicable to SMT due to the overlapping which implies a search involving complex calculations. The remaining three possibilities (clipping, TR and ACE) are investigated for SMT

scheme. All three possibilities combine time domain clipping with some additional signal processing either in the transmitter or in the receiver. First the simplest method is described where time domain clipping is applied to the transmit signal and an iterative scheme is used in the receiver to mitigated the introduced nonlinear distortions in the receiver. Next the TR technique is shown, where some subcarriers are allocated for PAPR reduction purposes leading to loss in data rate. Finally the ACE technique [Krongold2003] is presented where the outer points of the constellation are allowed to be enlarged dynamically. Both TR and ACE require an increase of average power.

5.5.1 Transmitter oriented iterative PAPR reduction for FBMC

In this section we focus on methods which can be used in the transmitter to reduce the PAPR of the transmitted signal, and the receiver side can be left unaltered without performance degradation. In system identification multisines are often used as measurement signal where a similar PAPR reduction is required. The main difference is that while in measurement the amplitude and phase of the sines are used for evaluation purposes, in wireless communication the amplitude and phase carries the data. In system identification a clipping aided iterative scheme has been developed to reduce the PAPR of multisines, presented in [Ouderaa1988]. A similar repeated clipping and filtering for OFDM was developed in [Armstrong2002], which can significantly reduce the PAPR but introduces significant amount of nonlinear distortion. Based on both ideas, incorporating their advantages, a similar algorithm suitable for FBMC is presented in this section.

The general block diagram of the transmitter oriented PAPR-reduction scheme is presented in Fig. 1. Extra signal processing blocks are added to the signal path prior to transmission. Following a conventional FBMC modulation of the symbols X, the PAPR of the generated FBMC signal s is measured. If it is below the predefined limit, it can be transmitted. If the amplitude is larger, clipping is applied. After clipping, the signal s^c is demodulated. The demodulated symbols X^c are then processed using a special selection and processing algorithm. Then the new symbols X^{new} are modulated again and the PAPR of the signal s^{new} measured. This process is repeated until the desired PAPR is reached or no reduction in the PAPR is achieved. After the iteration the signal s^{out} is used to form the analogue transmission signal.

The basic idea of the transmitter oriented iterative PAPR reduction for FBMC with clipping is depicted in Fig. 5-18.

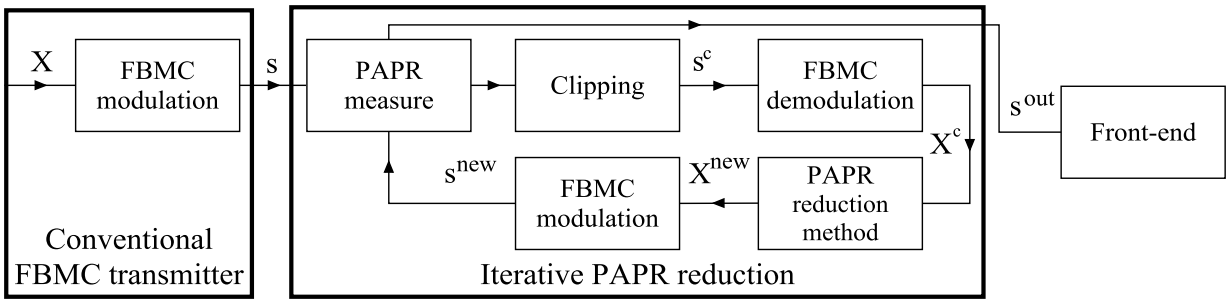

Figure 5-18: Block diagram of the clipping-based transmitter oriented iterative PAPR-reduction scheme for FBMC.

5.5.2 Tone reservation

As in OFDM the TR method can be applied to reduce the PAPR of FBMC signals as well. The idea is to reserve a certain number of subcarriers called Peak Reduction Tones (PRT) for PAPR-reduction, i.e. these are not used for data transmission. The TR technique can be applied in numerous ways, as shown in [Mroue2010].

In this thesis the clipping-based TR is applied, in which the clipping is applied to the time domain signal s to get the clipped signal s^c. The clipped signal is demodulated to retrieve complex modulation

symbols X^c effected by clipping. The data subcarriers are restored to their original state, while the PRTs are left unchanged to form X^{new}. Finally, modulation is applied to X^{new} to get the new time domain signal s^{new}. If this signal does not satisfy the PAPR criterion, $s = s^{new}$ is set and the next iteration is started. Basically the nonlinear noise is kept on the PRTs only, data carriers remain unchanged which leads to a peak regrowth when s^{new} is formed. The disadvantage of this technique is that the data rate is reduced, in correspondence with the number of the number of applied PRTs.

5.5.3 Active constellation extension

ACE was proposed by Krongold and Jones [Krongold2003] for PAPR-reduction. The idea behind the ACE technique is that the outer constellation points of the constellation alphabet *A* can be dynamically extended outwards of the original constellation, such that the PAPR of the data block is reduced [Krongold2003].

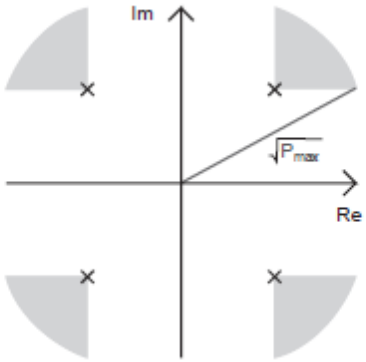

Figure 5-19. Extension regions for QPSK

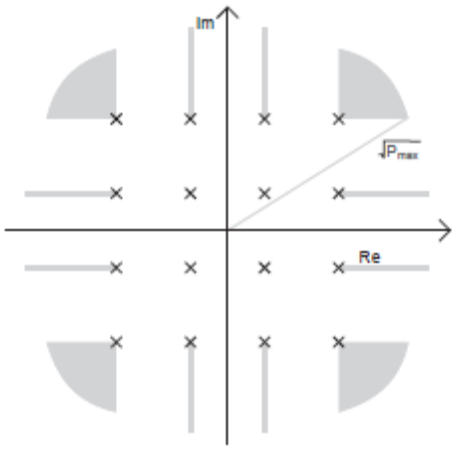

Figure 5-20. Extension regions for 16-QAM

Clipping-based ACE method starts with the time domain signal s. Following clipping, the signal s^c is demodulated to get X^c. After the demodulation the constraints are applied to the constellation, so that the constellation points are allowed to penetrate areas only which do not result in BER degradation. Other demodulated symbols are set to their original value.

For QPSK constellation the shaded area on Fig. 5-19 shows the region of the allowed extension. The figure also shows the restrictions to be made on constellation points regarding the maximal transmit power P_{max}. With these restrictions applied to the set X^c, X^{new} is obtained. Following a modulation, the new time domain signal s^{new} is formed. If the desired PAPR criteria is not met, $s = s^{new}$ is set and the next iteration is started again.

For higher order modulations the initial conditions and extension criteria are more complex. Figure 5-20. shows the extension regions for 16-QAM modulation. The figure shows that only the outer constellation points can be extended without a degradation of the system performance. Also while the corner points can be extended to a larger territory, the non-corner points can only be extended along a line. So the distorted modulation values X^c which fall outside the constellation and originate from an outer point -- but not from a corner point -- must be rotated to fall on the given line.

The advantage of ACE is that it does not require the transmission of additional information, nor does it decrease the data rate so the receiver can remain unchanged. As disadvantage, this method requires increased power for transmission of a data since the extended constellation points represent a carrier with higher amplitude than the original one. Another disadvantage of ACE is that no soft decision based detection can be applied due to distorted constellation points.

5.5.4 Joint use of TR and ACE

TR and ACE can be used simultaneously, since the two methods are independent of each other. TR acts on the PRTs and leave the data carrying subcarriers unchanged, while ACE modifies only the data carrying subcarriers leaving the PRTs unchanged. A certain number of carriers are reserved as in the TR method. This method leads to a PAPR-reduction with fast convergence but with the disadvantages of TR and ACE appearing at the same time: it leads to data rate loss and it requires extra transmission power.

5.5.5 Receiver oriented iterative PAPR reduction for FBMC

Another approach is to move the majority of the signal processing to the receiver side. The transmission signal is clipped and transmitted. In real-life systems not all subcarriers are used for data transmission. Usually the DC subcarrier and some carriers on the edge of the transmission band are not used due to technical difficulties and guard band purposes in the spectrum. Clipping introduces nonlinear distortions in the entire baseband, so the originally unused subcarriers will contain additional components introduced by clipping. This also negatively affects the spectral behaviour of the transmission signal i.e. leakage will appear. These additional components have to be suppressed. Digital filtering is not sufficient to suppress the clipping components on the unused subcarriers and analogue filtering introduces modulation errors. Instead of filtering, the clipped transmit signal is demodulated again. The modulation values for each symbol of the used subcarriers are selected and the unused subcarriers are set to zero and then the modulation procedure is repeated. The described modification of FBMC transmitter can be seen in Fig. 5-21.

Figure 5-21. Modified FBMC transmitter with clipping and filtering of the unused subcarriers

The nonlinear distortion term negatively affects the demodulation procedure on the receiver side. An iterative decoding scheme using the *Turbo Principle* to mitigate the distortion term was developed for OFDM \cite{soft} which was then applied for FBMC [kollar2012]. The disadvantage of the scheme is that it requires extensive calculations due to the iterative soft demapping and decoding procedure. The convergence of this scheme can be simply shown and analysed with the aid of EXIT charts [Brink2001].

The basic block diagram of the Bussgang Noise Cancelation (BNC) iterative detector for clipped FBMC signals is shown in Fig. 5-22. Detailed analysis and analytical formulas can be found in [kollar2012].

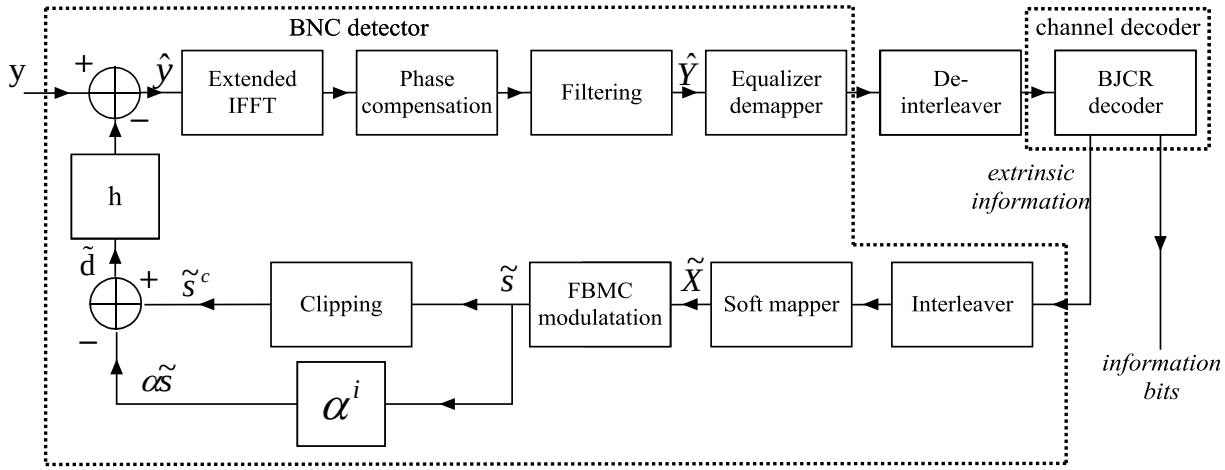

Figure 5-22 BNC scheme for clipped FBMC signals

Bit Error Rate (BER) performance over additive white Gaussian channel with a clipping ratio of 1 dB can be seen in Fig. 5-23. 16-QAM modulation was used for 768 subcarriers of the available 1024. The bits were encoded using a ½ rate convolutional encoder. With iterative compensation the system performance can be improved, above a certain noise level the BER results approach the performance of the case without clipping.

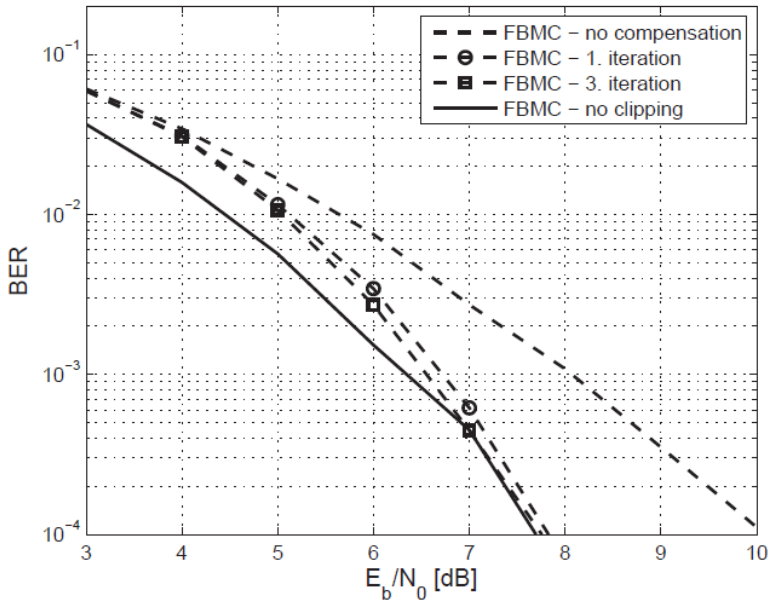

Figure 5-23 BER of the BNC receiver for FBMC signalling over AWGN channel

5.5.6 Simulation results

In this section simulation result are parented for the previously described PAPR-reduction methods in case of FBMC signals. During the simulations N=1024 carriers were implemented, from which 768 were used with 16-QAM modulation. In case of TR, 10% of the subcarriers were used as PRTs. In Fig. 5-24 the results of ACE, TR, ACE & TR and simple clipping with filtering are presented with a target PAPR of 3 dB over the number of iterations. In Fig. 5-25 the same parameters are used, with the only difference of the target PAPR for clipping being 1 dB in this case. It can be observed that for both cases the clipping with additional filtering provides the best performance. The price is the high computation complexity of the applied BNC receiver. The TR technique achieves the smallest PAPR

gain, the performance is not strongly dependent on the chosen clipping level. ACE outperforms TR in both cases, with a performance affected by the chosen clipping ratio. The joint use of TR & ACE outperforms the cases where only ACE or TR is used. The performance of clipping with filtering can reach up to 1.5 dB by the joint use of TR and ACE after the third iteration.

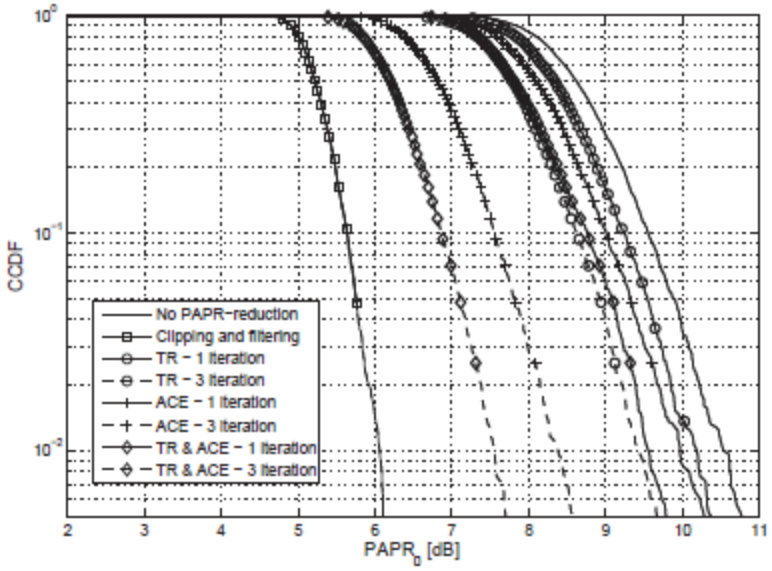

Figure 5-24. Comparison of the various PAPR-reduction techniques using 3 dB clipping.

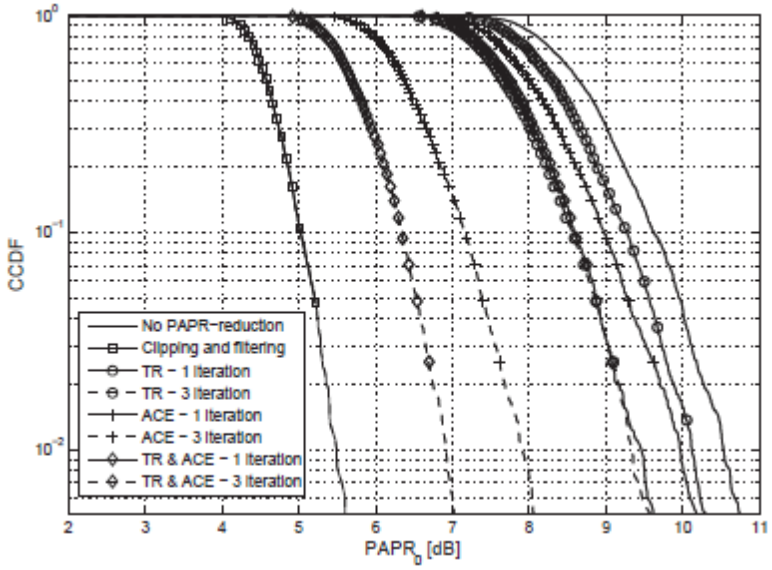

Figure 5-25. Comparison of the various PAPR-reduction techniques using 1 dB clipping.

Clipping-based PAPR-reduction schemes suitable for FBMC were presented. It has been shown that the FBMC signal also has a large PAPR. We have presented transmitter and receiver oriented iterative schemes which can be applied to FBMC without considerable performance degradation. The PAPR-reduction schemes were compared through simulations.

A summary and comparison of the advantages and disadvantages of the presented schemes are given in Table 5-2 by means of transmitter (Tx) and receiver (Rx) complexity, data rate loss, constellation distortion and power increase. Depending on the specific application requirements, the most suitable

PAPR-reduction technique can be chosen. As a future work the tradeoff between the power increase and the PAPR-reduction must be investigated. A possible dynamic setting of the clipping level should also be analysed.

Table 5-2 Comparison of the presented clipping based PAPR-reduction methods for FBMC.

PAPR-reduction Technique	Complexity	Data Rate Loss	Constellation Distortion	Power Increase
TR	Tx: moderate	Yes	No	Yes
ACE	Tx: high	No	Yes	Yes
TR+ACE	Tx: high	Yes	Yes	Yes
Clipping and filtering + BNC	Tx: low, Rx: high	No	Yes	No

5.6 Conclusions

We have proposed an FBMC-based physical layer waveform that complies with the tight regulatory ACLR requirements that are foreseen for opportunistic TVWS operation. As the proof-of-concept studies assume an FBMC-based physical layer, practical signal processing algorithms have also been presented and analysed for synchronization, channel equalization and mitigation of PA-induced nonlinear distortion. FBMC is very well suited to meet the stringent ACLR requirements imposed by the current regulations. It's extremely low side lobe leakage makes it an ideal candidate for opportunistic applications. However, care needs to be exercised not to compromise the ACLR properties in a practical system by introducing excessive nonlinear distortions. Controlling the PAPR of the transmitted signal is an efficient means of limiting possible distortions. In this chapter, three practical PAPR control schemes have been presented. We have also presented equalization schemes that can cope with channels exhibiting significant frequency dispersion (e.g. in the QoSMOS long-range scenarios). The simulation results confirm that, although FBMC is more complex than OFDM and the long temporal support of FBMC symbols poses challenges in the algorithm design, these difficulties can be managed and adequate performance is achievable over realistic wireless channels.

Potential contribution to standardization activities is foreseen based on the research results on lower ACLR and synchronization results. Lowering PAPR in FBMC is also a potential standardization contribution.

6 Case study: concept of an FBMC-based PHY for cognitive TVWS scenario

When it comes to the proof-of-concept implementation, both GFDM and FBMC/SMT could provide adequate suppression of adjacent-channel leakage. However, considering the fact that implementation challenges of FBMC/SMT are better explored in the open literature, and the theory is developed (mostly in the wireline context, but the wireless applications are also emerging), FBMC/SMT seems to offer a reasonable compromise. Therefore, QoSMOS demonstrations and proof-of-concept studies will include an FBMC/SMT-based physical layer. This chapter gives an overview on the progress of the hardware development and baseband/radio frequency (RF) interoperation aspects for the proof-of-concept. A RF impairment analysis of the selected FBMC waveform is also presented. The considerations carried out here complement the information given in [D7.2].

6.1 Concept overview, requirements

The PHY layer hardware concept is portrayed in Figure 6-1. It consists of several modules: the baseband board, the RF transmitter front-end, and up to two RF receiver front-ends. The digital signal processing as well as the hardware (re)configuration is performed by the baseband board, which includes an FPGA, an analogue-to-digital converter (ADC), and a digital-to-analogue converter (DAC). The analogue signal processing is performed by the front-end boards. This includes the frequency conversion, amplification, and filtering of the received signals and the signals to be transmitted, respectively.

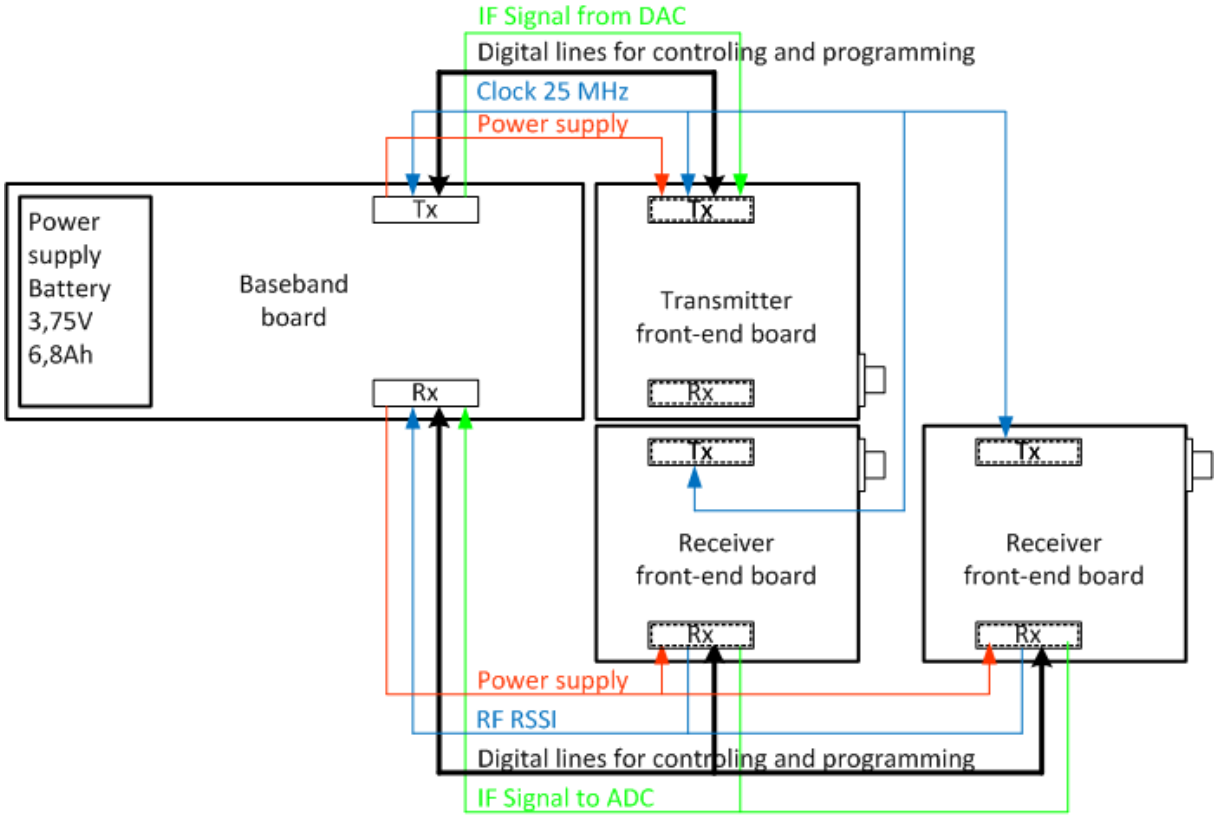

Figure 6-1: Schematic view of the hardware concept consisting of a baseband board, a transmitter front-end, and two receiver front-ends

A detailed description of the hardware concept as seen in Figure 6-1 and the hardware implementation can be found in [D7.2], as this is the basis for the 2nd Proof-of-Concept demonstration. In the following sections, a general view on the hardware concept and the requirements are given that eventually led to the concept selected.

6.2 RF Front-End Concepts

A preliminary RF transceiver front-end architecture has already been proposed in [D4.2]. To exploit a wide frequency region, the architecture is based on multiple branches, each covering a single frequency band, between which can be chosen using a switch. The main drawback of this approach is the high amount of components required.

To reduce the number of single components, a reconfigurable architecture is required, covering the whole frequency region that is supposed to be exploited. In the following subsection, an RF front-end architecture is discussed that consists of a single reconfigurable RF branch. Based on this approach a further architecture is proposed that allows for aggregation of two spectral white spaces. These white spaces can be arbitrarily distributed over the whole frequency region ("spectrum aggregation").

6.2.1 RF Receiver Front-End

Figure 6-2 shows the schematic view of the reconfigurable RF receiver front-end that has been designed in the QoSMOS project. The architecture of this receiver RF front-end is based on a super heterodyne architecture with a single IF stage.

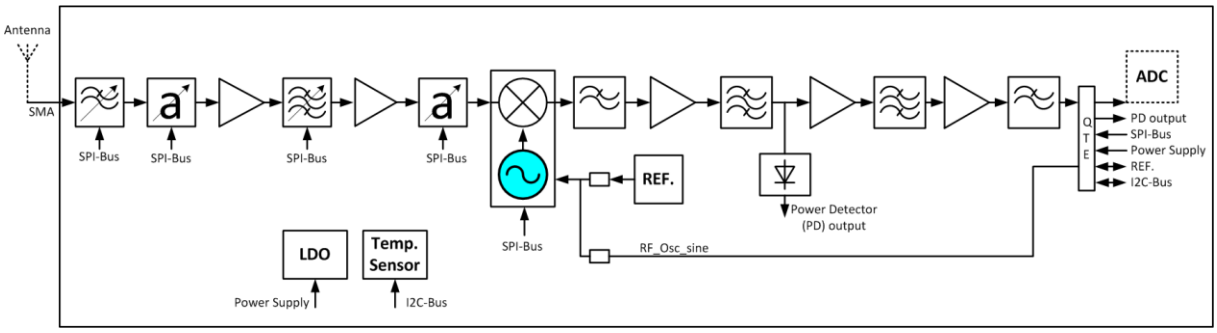

Figure 6-2: Schematic view of a reconfigurable RF receiver front-end

The components of this RF receiver front-end are:

- tuneable low pass filter
- tuneable band pass filter
- low noise amplifier
- digital step attenuator
- synthesizer/voltage controlled oscillator with mixer
- IF filter (SAW)
- broadband amplifier
- Power detector
- Reference frequency generator (TCXO)
- Temperature sensor
- Low drop out voltage regulator

The external Interfaces of this RF receiver front-end are the following:

- SMA connector for RF input
- Pin connector (QTE/QSE) for power supply, SPI Bus, I2C Bus and external reference clock

The RF signal is received by the antenna and filtered with the tLPF that serves as image rejection filter. After this filter the signal passes the digital step attenuator (DSA) that helps to prevent overload and distortion. The signal is then amplified by a low-noise amplifier (LNA) and fed to a tuneable band pass filter (tBPF) that serves as pre-selection filter. The band-limited signal passes another low noise amplifier and DSA to appropriately adjust the signal level. The signal is then down-converted to the intermediate frequency (IF) band and amplified and filtered by two SAW filter and low pass filter these serve as an anti-aliasing filter (AAF) before the IF signal is fed to an analogue-digital converter (ADC).

The gain can be adjusted in the RF part. There are two digital step attenuators that can be used for automatic gain control. The second stage DSA can be used also for temperature compensation. The design contains an external power detector that delivers an analogue voltage as measure of the received power to the baseband board.

As seen in Figure 6-2, three components are reconfigurable in terms of its centre frequency: the tLPF, the tBPF and the local oscillator (LO). These components are programmable via a 3-wire serial bus interface.

6.2.2 RF Transmitter Front-End

A schematic view of the reconfigurable RF transmitter front-end is presented in Figure 6-3.

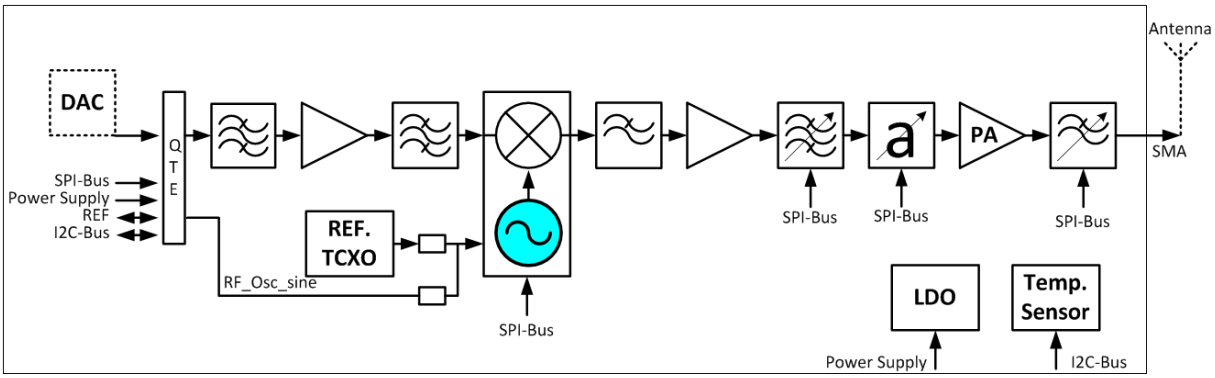

Figure 6-3: Schematic view of the reconfigurable RF transmitter front-end

The main components of this RF transmitter front-end are:

- tuneable low pass filter
- tuneable band pass filter
- power amplifier
- digital step attenuator
- synthesizer/voltage controlled oscillator with mixer
- IF filter (SAW)
- broadband amplifier
- Reference frequency generator (TCXO)
- Temperature sensor
- Low drop out voltage regulator

The external Interfaces of this RF transmitter front-end are as follows:

- SMA connector for RF output

- Pin connector (QTE/QSE) for power supply, SPI Bus, I2C Bus, external reference clock

The IF-Signal generated by a digital-analogue converter (DAC) passes an AAF and amplifier, before it is up-converted to the RF region. The RF signal is filtered with the low pass filter and amplified using a fixed gain amplifier and fed to the tBPF that serves as pre-selector filter. The gain can be adjusted in the RF part with the digital step attenuator (DSA). Then the signal is amplified using the power amplifier (PA), passes the tLPF that serves as the out-of-band rejection filter, and is eventually fed to the antenna.

As seen in Figure 6-2, three components are reconfigurable in terms of its centre frequency: the tLPF, the tBPF and the local oscillator (LO). These components are programmable via a 3-wire serial bus interface.

6.2.3 RF Front-End Specifications

Table 6-1 and 6-2 show the main specifications of the RF front-end hardware. The specifications are based on the 2nd Proof-of-Concept demonstration outlined in [D7.1] and discussed in detail in [D7.2].

Parameter	specification	Condition
Electrical		
RF Frequency range	470 MHz to 860 MHz	
INPUT/OUTPUT Return loss	-10 dB	50 Ohm
IF center frequency	280 MHz	With 40 MHz band width
Gain	ca. 30 dB	Without AGC
Gain Adjustment range	6 dB	In 0.25 dB steps for temperature compensation
AGC Adjustment range	31 dB	In 0.25 dB steps
Noise Figure	< 6 dB	Max. Gain
Dynamic range	-87 dB	
Sensitivity	-90 dBm	10 dB SNR
Oscillator		
LO	High side	For whole frequency band
LO frequency	750 MHz to 1140 MHz	
Phase noise	-109 dBc/H	@100kHz
Mechanical		
Physical dimensions	68 mm x 77 mm	
Interface		
RF Input	SMA Female	
Baseband-Board	QTE/QSE connector	IF IN, Power supply, control
Operating Conditions		
Temperature	-40˚C to +85˚C	
Power supply	3.7 V	Single Battery via SAMTEC connector
Current consumption	ca. 470 mA	
Reference Frequency		
Reference frequency on Board TCXO	25 MHz	External via SAMTEC connector

Reference input level	800 mV p-p	

Table 6-1: RF receiver front-end specification

Parameter	specification	Condition
Electrical		
RF Frequency range	470 MHz to 860 MHz	
INPUT/OUTPUT return loss	-10 dB	
IF center Frequency	280 MHz	With 40 MHz band width
Output power	+17 dBm	With the maximal gain ca. 22 dB
Output IP3	tbd	2 tones
Gain adjustment	6 dB	In 0.25 dB steps for temperature compensation
Oscillator		
LO	High side	For whole frequency band
LO frequency	750 MHz to 1140 MHz	
Phase noise	-109 dBc/Hz	@100kHz
Mechanical		
Physical dimensions	68 mm x 77 mm	
Interface		
RF output	SMA Female	
Baseband-Board connector	QTE/QSE connector	IF IN, Power supply, control
Operating Conditions		
Temperature range	-40˚C to +85˚C	
Power supply	3.7 V	via SAMTEC connector
Current consumption	ca. 470 mA	
Reference Frequency		
Reference frequency	25 MHz	External via SAMTEC connector
Reference input level	800 mVpp	

Table 6-2: RF transmitter front-end specification

6.3 Power spectrum density considerations

The proposed FBMC waveform focuses on low out-of-band radiation. Nonlinear distortions, mainly caused by power amplifiers, are known to introduce spectrum growth in the adjacent bands. We have conducted a theoretical investigation on the expected ACLR performance of the proposed waveform. Currently, as our own measurement results are not yet available, we have to resort to the data sheet of the power amplifier module that has been chosen for the transmitter implementation. The part is RFPA0133, a programmable-gain integrated GaAs PA from RF Micro Devices [RFPA0133].

The data sheet provides output power vs. input power curves at 860 MHz. This rather limited characterization allows us to model the PA as a memoryless nonlinearity with no AM-PM conversion (as the phase characteristics are not known). Nevertheless, this analysis still provides some insight into the expected performance. The calculation follows the method outlined in [Banelli2000]. Provided the

nonlinear distortion function can be decomposed into a Bessel series [Kaye1972], one can estimate the output PSD based on the input PSD, if the input signal is approximately Gaussian. The PSD of the input FBMC signal is available either analytically or can be obtained using simulations, as presented in Chapter 5. Although the method in [Banelli2000] is originally proposed for OFDM signals, the underlying assumptions are also valid for FBMC/SMT signals, as the amplitude distribution of these modulation schemes is essentially the same. As we show, this analysis technique yields to good agreement with the simulation data also for the FBMC/SMT scheme.

The AM/AM characteristics of the selected PA module are approximated using a 5-term Bessel series approximation. The resulting output power vs. input power curve is shown in Figure 6-4, together with the measured curve, as taken from the data sheet.

To ensure a low level of nonlinear distortion products, back-off is applied to the amplifier. The input back-off (IBO) is defined as the ratio of the input saturation power and input mean power. We calculate the output PSD for different IBO values in order to determine the necessary back-off.

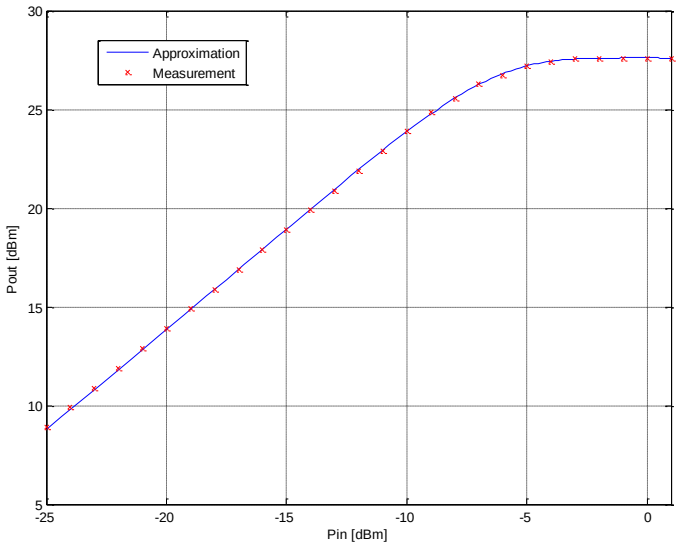

Figure 6-4: Bessel series fit of the RFPA0133 characteristics

The resulting SMT power spectrum density can be determined analytically. The output PSDs with FBMC/SMT signal with two different input back-off levels are shown in Figure 6-5. The analytic form is obtained by accounting for the useful signal and the dominating lowest-order distortion product. Simulation results are also shown for comparison. As seen in the figure, 20 dB input back-off yields to almost -50 dB ACLR (sufficient to meet the OFCOM mask), whereas with 25 dB back-off one can attain about -60 dB ACLR, which is sufficient to meet the regulatory constraints imposed by FCC. It should be noted that the above analysis yields the *average* PSD, and an analogue spectrum analyser wouldn't necessarily show the same PSD. According to the device data sheet, employing 20…25 dB input back-off would yield to an output average power of about +10…15 dBm which is less than the +17 dBm allowed by regulators.

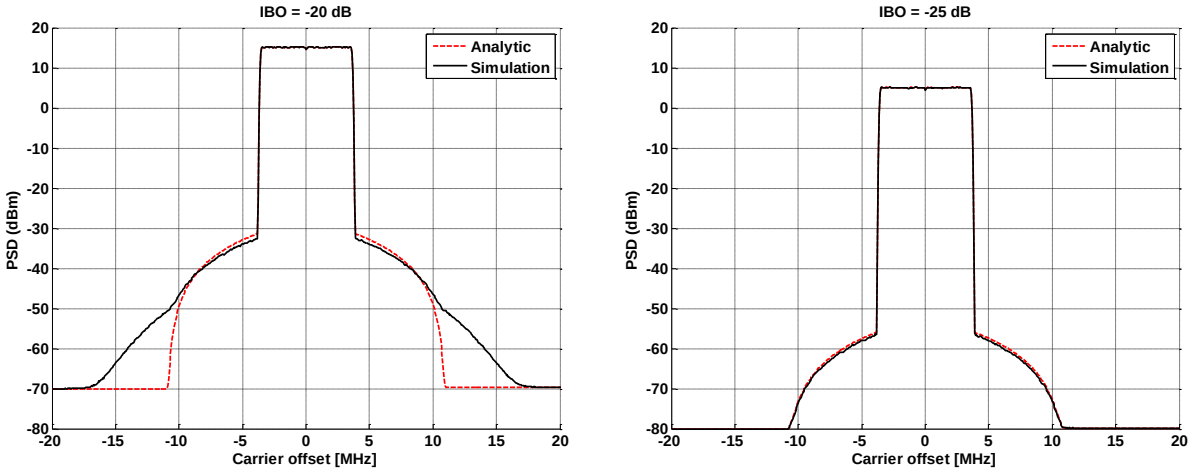

Figure 6-5: PSD of the distorted FBMC/SMT signal

This study demonstrates the feasibility of using FBMC/SMT with the selected RF PA module for a TVWS application. With appropriate back-off we can meet the strict ACLR requirements imposed by the regulators.

6.4 Conclusions

This chapter presented the selected RF architecture for the proof-of-concepts. Double-branch transceiver architecture was chosen, for which the critical RF specifications are also given. The architecture allows exploiting two arbitrarily chosen channels simultaneously, increasing therefore the capacity and the flexibility. A nonlinear distortion analysis of FBMC is also presented taking the characteristics of the selected PA module into account, in order to predict the amount of necessary back-off that guarantees the low adjacent channel leakage level required by the OFCOM specifications.

7 Conclusions and further work

This document is the final version of D4.2 and reports on the progress of identifying the most appropriate modulation schemes for a cognitive radio system operating in TV white spaces. It was demonstrated that filtered OFDM is not necessarily the best solution to address the currently known strict regulatory requirements regarding the adjacent channel leakage. It was also shown that multicarrier modulation schemes are best suited for this application, and common multicarrier parameter settings have been identified for the various QoSMOS scenarios.

Four, rather different approaches were proposed, starting from slightly modified OFDM schemes (windowed OFDM and IA-PFT) that can operate well with legacy systems, and two more general classes (FBMC/SMT and GFDM) that have the potential to meet the low adjacent-channel leakage requirements. Some implementation-related aspects were also addressed in conjunction with FBMC, especially topics in which FBMC is generally regarded as more complex or more difficult to handle than OFDM-based schemes: synchronization and channel equalization. We can conclude that it is now possible to reach lower ACLR levels and meet regulatory requirements. One of the conclusions we can derive from this work is that of all the four novel PHY designs proposed, FBMC is the most suitable at this point for implementation in CR TVWS scenarios.

Finally, the progress on the two-branch transceiver implementation has been presented, together with some considerations on the expected ACLR performance of the FBMC-based PHY that was selected for the proof of concepts.

Future work within the work package focuses primarily on the implementation aspects. Advanced detection techniques have not been considered in much detail for FBMC, neither the possibility of employing multiple antenna schemes to the presented modulation techniques in a TVWS setting. Sensing opportunistic signals is also of importance and needs to be studied even further.

8 References

[802.11af] IEEE 802.11af, TV white space study group af, Wireless Local Area Network (WLAN), http://www.ieee802.org/11/

[802.22] IEEE 802.22, Wireless Regional Area Networks ("WRANs"), http://www.ieee802.org/22/

[Armstrong2002] J. Armstrong, "Peak-to-average power reduction for OFDM by repeated clipping and frequency domain filtering," *Electronics Letters*, vol. 38, no. 5, pp. 246–247, 2002.

[Bader2010] F. Bader, M. Shaat, "Pilot Pattern Adaptation and Channel Estimation in MIMO WiMAX-like FBMC System," *Wireless and Mobile Communications (ICWMC), 2010*, pp.111-116

[Bader2011] F. Bader, M. Shaat, "Pilot Pattern Design for PUSC MIMO WiMAX-like Filter Banks Multicarrier System," *International Journal On Advances in Telecommunications*, Volume 4, Numbers 1 and 2, 2011, pp.156-165, Sept. 2011

[Banelli2000] P. Banelli and S. Cacopardi, "Theoretical analysis and performance of OFDM signals in nonlinear AWGN channels," IEEE. Trans. Communications, Vol. 48, No. 3, pp. 430-441, March 2000

[Barshanti2011] R.J. Barsanti and J. Larue, "Peak to average power ratio reduction for digital video broadcast T2," in *2011 Proceedings of IEEE Southeastcon*, Mar. 2011, pp. 117–121.

[Berg2011] V. Berg and D. Noguet, IEEE 1900.7 White Space Radio, *ACLR issues with OFDM for TVWS operation*, 2011-12-12/14; Scottsdale, AZ

[Bracewell99] R. E. Bracewell, *The Fourier transform and its applications*, McGraw-Hill, 1999

[Bran2005] S. Brandes, I. Cosovic and M. Schnell, "Reduction of out-of-band radiation in OFDM based overlay systems," *DySPAN 2005*, pp.662–665, Nov. 2005.

[Brink2001] S. ten Brink, "Convergence behavior of iteratively decoded parallel concatenated codes," *IEEE Trans. Commun.*, vol. 49, no. 10, pp. 1727–1737, 2001

[Chouinard2011] G. Chouinard, RF Mask Considerations, IEEE 802.22 Del-template, 2011-11-04

[Clark1972] A. Clark, ''Adaptive Detection with Intersymbol-Interference Cancellation for Distorted Digital Signals'', *IEEE Transactions on Communications*, Vol 20, No 3, Part 2, pp. 350 – 361, 1972

[D1.3] FP7-ICT-2009-4/248454, QoSMOS Deliverable D1.3, *QoSMOS initial system requirements*, Dec. 2010

[D2.3] FP7-ICT-2009-4/248454, QoSMOS Deliverable D2.4, *System specification and evaluation criteria*, Dec. 2011

[D4.1] FP7-ICT-2009-4/248454, QoSMOS Deliverable D4.1, *Transceiver architectures and requirements*, Aug. 2010

[D7.1] FP7-ICT-2009-4/248454, QoSMOS Deliverable D7.1, *QoSMOS Platform Architecture Definition (1/2)*, Dec. 2010

[D7.2] FP7-ICT-2009-4/248454, QoSMOS Deliverable D7.2, *QoSMOS Platform Architecture Definition (2/2)*, to be submitted, Dec. 2011

[Datta2011] R. Datta, G. Fettweis, Zs. Kollár and P. Horváth, ''FBMC and GFDM Interference Cancellation Schemes for Flexible Digital Radio PHY Design'', in *Proceedings of 14th Euromicro Conference on Digital System Design*, Sept. 2011.

[Djardin2007] R. Djardin, M. Colas, G. Gelle, "Comparison of iterative receivers mitigating the clipping noise of OFDM based system," *European Wireless Conference 2007*, April 2007.

[Farhang-Boroujeny2010] B. Farhang-Boroujeny and C. H. Yuen, "Cosine Modulated and Offset QAM Filter Bank Multicarrier Techniques: A Continuous-Time Prospect," *EURASIP Journal on Advances in Signal Processing*, May 2010.

[FCC1] FCC proposed rule, "*Unlicensed Operation in the TV Broadcast Bands*", US Federal Register Vol. 69, No.117, pp. 34103-34111, June 18, 2004.

[Fettweis2009] G. Fettweis, M. Krondorf and S. Bittner, "GFDM – General Frequency Division Multiplexing", in *Proceedings of IEEE 69th Vehicular Technology Conference (VTC Spring'09)*, 26-29 April 2009.

[Fort2003] A. Fort and W. Eberle, "Synchronization and AGC proposal for IEEE 802.11 a burst OFDM systems," *IEEE Global Telecommunications Conference, GLOBECOM '03*, Vol. 3, pp. 1335-1338, Dec 2003

[Freyens2011] B. P. Freyens, M. Loney, "Opportunities for White Space Usage in Australia", *2nd International Conference on Wireless Communications, Vehicular Technology, Information Theory and Aerospace in Electronic Systems Technology (Wireless VITAE)*, Chennai, India, March 2011.

[Fusco2009] T.Fusco, A. Petrella, M. Tanda, M, "Data-aided symbol timing and CFO synchronization for filter bank multicarrier systems," *IEEE Transactions on Wireless Communications*, Vol. 8, No. 5, pp. 2705-2715, May 2009

[Han2005] S. H. Han and J. H. Lee, "An Overview of Peak-to-average Power Ration Reduction Techniques for Multicarrier Transmission," *IEEE Trans. Wireless Communication*, pp. 56-65, April 2005.

[Hirosaki1981] B. Hirosaki, "An Orthogonally Multiplexed QAM System Using the Discrete Fourier Transform," *IEEE Transactions on Communications*, Vol. 29, No. 7, pp. 982-989, Jul 1981

[IEEE1999] IEEE, "*Supplement to IEEE Standard for Information technology—Telecommunications and information exchange between systems—Local and metropolitan area networks—Specific requirements—Part 11: Wireless LAN Medium Access Control (MAC) and Physical Layer (PHY) specifications: High-speed Physical Layer in the 5 GHz Band*", IEEE Std 802.11a-1999.

[Ihalainen2002] T. Ihalainen, T. Hidalgo-Stitz, M. Renfors, "On the performance of low-complexity ASCET-equalizer for a complex transmultiplexer in wireless mobile channel," *Proc. 7th Intl. OFDM-Workshop 2002*, Hamburg, Germany, Sept. 2002.

[Javaudin2003] J.-P. Javaudin, D. Lacroix, A. Rouxel, "Pilot-aided channel estimation for OFDM/OQAM," *IEEE Vehicular Technology Conference*, 2003., Vol. 3,

pp. 1581-1585

[Kang2007] S.W. Kang and K.H. Chang, “A novel channel estimation scheme for OFDM/OQAM-IOTA system,” *ETRI Journal*, Vol. 29, pp. 430–436, Aug. 2007.

[Kaye1972] A. Kaye, D. George and M. Eric, “Analysis and Compensation of Bandpass Nonlinearities for Communications,” IEEE Trans. Communications, Vol. 20, No. 5, pp. 965-972, Oct 1972

[Kollár2008] Zs. Kollár, M. Grossmann, and R. Thomä, “Convergence analysis of BNC turbo detection for clipped OFDM signalling.” *13th International OFDM-Workshop 2008, InOWo’08*, Hamburg, Germany, pages 241–245, August 2008.

[Kollar2010] Zs. Koll´ar and P. Horv´ath, “Modulation schemes for cognitive radio in white spaces,” *Radioengineering*, vol. 19, no. 4, pp. 511–517, Dec. 2010.

[Kollár2011a] Zs. Kollár, G. Péceli, and P. Horváth. “Iterative decision feedback equalization for FBMC systems,” *First International Conference on Advances in Cognitive Radio*, COCORA 2011, Budapest, Hungary, April 2011.

[Kollár2011b] Zsolt Kollár, Péter Horváth, “ Physical Layer Considerations for Cognitive Radio: Synchronization Point of View,” IEEE 73rd Vehicular Technology Conference: VTC2011-Spring, May 2011, Budapest, Hungary

[Kollar2012] Zs. Kollár and P. Horváth, “PAPR reduction of FBMC by clipping and its iterative compensation,” *Journal of Computer Networks and Communications*, vol. 2012, 2012.

[Krongold2003] B. S. Krongold and D. L. Jones, “PAPR Reduction in OFDM via Active Constellation Extension,” *IEEE Trans. Broadcasting*, Vol. 49, No. 3, Sept. 2003, pp. 258-268.

[Morelli2007] M. Morelli, C.-C.J. Kuo, M.-O. Pun, "Synchronization Techniques for Orthogonal Frequency Division Multiple Access (OFDMA): A Tutorial Review," *Proceedings of the IEEE*, Vol. 95, No. 7, pp.1394-1427, July 2007

[Mroue2010] M. Mroué, A. Nafkha, J. Palicot, Gavalda B., and N. Dagorne, “Performance and implementation evaluation of TR PAPR reduction methods for DVB-T2,” *International Journal of Digital Multimedia Broadcasting*, vol. 2010, pp. 2–4, Apr. 2010.

[Nicola2011] N. Michailow, M. Lentmaier, P. Rost and G. Fettweis, “Integration of a GFDM Secondary System in an OFDM Primary System”, in *Proceedings of Future Network and Mobile Summit (FuNeMs’11)* 2011, Warsaw, Poland.

[Noguet2011] D. Noguet, M. Gautier and V. Berg, “Advances in Opportunistic Radio Technologies for TVWS,” EURASIP Journal on Wireless Communications and Networking 2011, 2011:170 doi:10.1186/1687-1499-2011-170, Published: 15 November 2011

[OFCOM] *Digital dividend: cognitive access, statement on licence-exempting cognitive devices using interleaved spectrum*, OFCOM, July 2009

[Ouderaa1988] E. Van der Ouderaa, J. Schoukens, and J. Renneboog, "Peak factorminimization using a time-frequency domain swapping algorithm,"*Instrumentation and Measurement, IEEE Transactions on*, vol. 37,no. 1, pp. 145 –147, Mar. 1988.

[Petrella2009] A. Petrella, *Synchronization algorithms for FBMC systems*, [doctoral thesis], Università degli Studi di Napoli Federico II, 2009

[Rahim2009] M. U. Rahim, T. H. Stitz and M. Renfors, "Analysis of Clipping-Based PAPR-Reduction in Multicarrier Systems," *IEEE 69th Vehicular Technology Conference Spring 2009*, 26-29 April 2009.

[Rappaport1996] Th. S. Rappaport, *Wireless Communications: Principles and Practice*, Prentice Hall, 1996.

[RFPA0133] RFPA0133, *3 TO 5 V PROGRAMMABLE GAIN HIGH EFFICIENCY POWER AMPLIFIER* (data sheet), www.rfmd.com

[SE43] Report from CEPT to the European Commission in response to the Mandate on "*The identification of common and minimal (least restrictive) technical conditions for 790 - 862 MHz for the digital dividend in the European Union*", CEPT report 30 http://www.erodocdb.dk/Docs/doc98/official/pdf/CEPTREP030.PDF, October 2009.

[Schwartz90] M. Schwartz, *Information transmission, modulation, and noise*, McGraw-Hill, 1990

[Skrzypczak2006] A. Skrzypczak, J-P. Javaudin, P. Siohan, "Reduction of the Peak-to-Average Power Ratio for the OFDM/OQAM Modulation," *IEEE 63rd Vehicular Technology Conference, Spring 2006*, pp.2018-2022, 7-10 May 2006

[Stitz2010] T. H. Stitz, T. Ihalainen, A. Viholainen, and M. Renfors, "Pilot-Based Synchronization and Equalization in Filter Bank Multicarrier Communications," *EURASIP Journal on Advances in Signal Processing*, vol. 2010, pp. 1-19, 2010.

[TS36.201] 3GPP, TS 36.201 (V9.1.0), *LTE Physical Layer - General Description*, Mar. 2010.

[TS36.211] 3GPP, TS 36.211 (V9.1.0), *Physical channels and modulation*, Mar. 2010.

[Waterschoot2010] T. van Waterschoot, V. Le Nir, J. Duplicy, M. Moonen, "Analytical Expressions for the Power Spectral Density of CP-OFDM and ZP-OFDM Signals", *IEEE Signal Processing Letters*, vol. 17, no. 4, pp. 371-374, April 2010.

[Yam2004] H. Yamaguchi, "Active interference cancellation technique for MB-OFDM cognitive radio," *Microwave conference 2004*, pp. 1105–1108, Oct. 2004.

[Yoon2008] T. Yoon, S. Im, S. Hwang, H. Choi, "Pilot Structure for High Data Rate in OFDM/OQAM-IOTA System," *IEEE Vehicular Technology Conference, VTC 2008-Fall*, Sept. 2008.